Universidade do Porto

Faculdade de Engenharia da Universidade do Porto

Instituto de Ciências Biomédicas Abel Salazar

Instituto de Engenharia Biomédica

Modeling the mechanics of EMT: effect of variations in extracellular matrix viscoelastic properties

Diana Isabel Pereira Saraiva

Masters in Bioengineering – Molecular Biotechnology

Porto, July 2015

Modeling the mechanics of EMT:
effect of variations in extracellular matrix viscoelastic properties

Diana Isabel Pereira Saraiva

Thesis for Masters in Bioengineering

FEUP – Faculdade de Engenharia da Universidade do Porto

ICBAS-UP – Instituto de Ciências Biomédicas de Abel Salazar

Supervisor:

Cristina Barrias, Ph.D. **i3S/INEB**

Co-supervisor:

Sílvia Bidarra, Ph.D. **i3S/INEB**

i3S – Instituto de Investigação e Inovação em Saúde

INEB - Instituto de Engenharia Biomédica, Universidade do Porto

ABSTRACT

Epithelial-to-mesenchymal transition (EMT) is a process strongly implicated in cancer progression and dissemination. EMT and its reversion (mesenchymal-to-epithelial transition, MET) confer cell plasticity, allowing cell dispersion during development and cancer dissemination. Cancer invading cells display EMT-related features such as mesenchymal phenotype and/or detachment and movement towards the stroma, expression of vimentin (M marker), and loss of functional E-cadherin (E marker). Conversely, when cancer cells successfully establish metastasis at secondary sites, they re-acquire E markers while maintaining aggressive tumour features. The tumour extracellular matrix (ECM), which undergoes drastic alterations in composition/organization during cancer progression, has been shown to play a critical role in this process, namely by promoting, inhibiting, or reverting EMT. Yet, underlying mechanisms are still poorly understood, largely due to the lack of adequate dynamic models to study cell-matrix crosstalk.

The aim of this work was to develop a new 3D *in vitro* model to dissect the effect of matrix stiffness on EMT. To set up this model, a near-normal mammary epithelial cell line (EpH4) was combined with a bioengineered 3D matrix of alginate functionalized with cell-adhesive RGD peptides.

In the first part of the thesis, a method for dynamically switch matrix mechanical properties *in situ* was established. Using $CaCl_2$ or $SrCl_2$ as external crosslinking agents, at optimized concentrations and incubation times, the original stiffness of acellular or cell-laden hydrogels (3D culture) could be significantly increased. This way, the hydrogel's storage moduli (G') could be changed, ranging from that of normal mammary tissue (around 200 Pa) to that of malignant mammary tissues (around 4000 Pa). The inverse process, i.e. hydrogel softening, was promoted using sodium citrate as chelating agent, and cycles of hydrogels stiffening followed by softening or vice-versa were also settled. It was demonstrated that incubation of hydrogel-entrapped cells in stiffening and softening agents did not significantly impair their metabolic activity.

In the second part of the thesis, the behaviour of EpH4 cells cultured under 3D conditions in control hydrogels was evaluated. 3D culture of EpH4 cells within soft RGD-alginate matrices recapitulated epithelial morphogenesis. Single EpH4 cells were able to proliferate forming spheroids by clonal-growth, which maturated into organotypic mammary accini, presenting typical features as growth arrest, lumenization and apicobasal polarization. The maintenance of mRNA expression levels of typical E markers (*CDH1*, *Ocln*), with no up-regulation in expression of M markers (*CDH2*) and

EMT inducers (*Zeb2*), demonstrated that 3D culture within soft RGD-alginate matrices did not induce EMT *per se.*

Finally, in the last part of the thesis, the effect of *in situ* matrix stiffening on 3D cultured EpH4 cells was investigated. Cell-laden RGD-alginate hydrogels were stiffened with $SrCl_2$, to increase their storage modulus from ca. 250 Pa to ca. 4300 Pa. Stiffening was promoted immediately after entrapment (at day 1) or only after spheroids formation (at day 10). In the later case, no significant differences were observed between control and stiffened samples. Yet, when matrices were stiffened at the onset of the 3D culture, some differences were observed, namely in terms of cell proliferation and spheroids formation/size, which were decreased in stiffened matrices. Some phenotypic differences were also detected. At protein level, there was an apparent slight decrease of E-cadherin expression/function and a slight increase in vimentin expression. At mRNA level, cells in stiffened matrices had slight increased expression of *CDH1* and *CDH2* but decreased expression of *Ocln* and *Mgat3* (E-associated marker). Expression of *Zeb2* and *Id2* (negative regulator of TGFβ1–induced EMT) remained unchanged. Taken together, these results demonstrate that matrix stiffing effectively affected the overall behaviour of 3D-cultured EpH4 cells, and may eventually suggest a partial transition to a more M-like state. No differences in MMP2 and MMP9 expression between control and stiffened matrices were detected in both experimental set-ups.

Although the experiments performed in this final part of the thesis are still very preliminary, and no consistent conclusions on stiffness-driven EMT occurrence can be taken at this stage, our results demonstrate the versatility of the proposed 3D model. In the future, this *in vitro* platform is expected to provide a valuable tool to improve current knowledge on the role of ECM properties on EMT/MET, and may help in the identification of putative targets for more effective anti-cancer therapies.

RESUMO

Durante a transição epitélio-mesenquimal (EMT), as células epiteliais adquirem características mesenquimais, como o aumento da expressão de vimentina e a perda de caderina-E funcional. Adicionalmente, a adesão entre células e com a matriz extracelular é enfraquecida, o que leva as células a destacarem-se da membrana basal e a movimentarem-se em direcção ao estroma, aumentando a sua capacidade de invasão. Este processo de EMT está envolvido na progressão e disseminação tumoral, sendo que as células tumorais epiteliais também adquirem um fenótipo mesenquimal, podendo invadir o tecido e formar metástases. Quando as metástases se estabelecem em nichos secundários, o processo inverso – transição mesenquimal para epitelial (MET) ocorre e as células readquirem marcadores epiteliais, como a expressão de caderina-E, mantendo outras características tumorais profundamente agressivas. A matriz extracelular (ECM) tumoral sofre grandes alterações na sua composição e organização durante a progressão tumoral. Foi descrito que a ECM tem um papel crítico neste processo, nomeadamente por promover, inibir ou reverter a EMT. No entanto, os mecanismos pelos quais esta influência ocorre ainda não são conhecidos, devido, principalmente, à falta de modelos dinâmicos adequados para estudar as interacções entre a matriz e as células.

O principal objectivo deste trabalho foi desenvolver um modelo 3D *in vitro* para caracterizar o efeito das propriedades mecânicas da ECM, designadamente, o efeito do aumento da rigidez da matriz *in situ* em EMT. Para tal, uma linha celular epitelial mamária (EpH4) foi combinada com uma matriz 3D de alginato funcionalizado com péptidos que promovem a adesão celular (RGD).

Em primeiro lugar, foi estabelecido um método *in situ* para alterar dinamicamente as propriedades mecânicas da matriz. Com $CaCl_2$ ou $SrCl_2$, como agentes de *crosslinking* externo, a rigidez dos hidrogéis acelulares e celulares (3D) foi aumentada, desde níveis semelhantes aos do tecido mamário normal (~200 Pa) até a níveis de rigidez dos tecidos mamários malignos (~4000 Pa). O processo inverso, isto é, a diminuição da rigidez do hidrogel, foi promovido com citrato de sódio que actua como um agente quelante. Foram ainda estabelecidos dois ciclos de aumento e diminuição da rigidez ou vice-versa. Foi também demonstrado que a incubação de hidrogéis celulares nestes agentes não altera significativamente a actividade metabólica celular.

Na segunda parte da tese, foi avaliado o comportamento das células EpH4 em 3D. As células EpH4 numa cultura 3D de alginato-RGD são capazes de manter a morfogénese epitelial: proliferam e formam esferóides que maturam em estruturas mamárias típicas denominadas de *acinares.* Estas estruturas evidenciaram uma fase

de *plateau* no crescimento celular, lumenização e polarização apicobasal - características típicas encontradas *in vivo*. A manutenção dos níveis de mRNA de marcadores E (*CDH1* e *Ocln*), a reduzida expressão de marcadores M (*CDH2*) e de indutores de EMT (*Zeb2*), demonstraram que a matriz de alginato-RGD por si só não induz EMT nas células EpH4.

Finalmente, na terceira parte da tese, foi observado o efeito do aumento da rigidez da matriz *in situ*. A matriz com células EpH4 foi enrijecida com $SrCl_2$ e foi possível aumentar a rigidez desde ~250 Pa até ~4300 Pa. O acréscimo da rigidez da matriz ocorreu imediatamente a seguir ao aprisionamento celular na matriz ou só ao dia 10, após a formação dos esferóides. No último caso, não foram detectadas diferenças significativas entre as amostras controlo e as enrijecidas. No entanto, matrizes enrijecidas ao dia 1 tinham a formação e o tamanho dos esferóides reduzidos, menor proliferação celular, decréscimo na expressão de caderina-E e ligeiro aumento na expressão de vimentina (ao nível da proteína). Ao nível do mRNA, células em matrizes enrijecidas tinham expressão aumentada de *CDH1 e CDH2* e expressão diminuída de *Ocln* e *Mgat3* (marcador associado ao fenótipo E). A expressão de *Zeb2 e Id2* (regulador negativo da indução de EMT por TGFβ1) permaneceu igual. Resumindo, estes resultados demonstram que o aumento da rigidez da matriz afecta o comportamento das células EpH4 em 3D, sugerindo uma possível transição parcial para um fenótipo mais mesenquimal. Não foram detectadas diferenças na secreção de MMP2 e MMP9 entre amostras controlo e enrijecidas, em ambas as experiências.

Apesar das experiências efectuadas na parte final da tese ainda serem preliminares e de não haver conclusões consistentes sobre o efeito da rigidez em EMT, os nossos resultados demonstram a versatilidade do modelo 3D proposto. No futuro, espera-se que esta plataforma 3D sirva para melhorar o conhecimento do papel das propriedades da ECM em EMT/MET, e para identificar alvos para terapias anti-tumorais mais eficazes.

ACKNOWLEDGEMENTS

To my supervisor, Dr. Cristina Barrias, I would like to acknowledge the opportunity given to work on this project. I am also thankful for her constant support and motivation and for creating an environment where I was thrilled to go beyond and push myself. I have to thanks to her for all that she taught me and for increasing my interest in following a scientific career.

I would also like to thank to my co-supervisor, Dr. Sílvia Bidarra, for always being there for me, for teaching all the techniques, for answering all my doubts and for her patience and advice. A most sincere acknowledge for her support in the final days of this project.

I am also thankful to Dr. Patricia Oliveira and Dr. Carla Oliveira from the Expression Regulation in Cancer group at IPATIMUP for all the contributions provided to this work.

To everyone in Biocarrier group, that welcomed me and helped me throughout the development of this project.

A special thanks to my best friends, Sarah, Filipe e Catarina that are always there for me and helped me in yet another important stage of my life. Also, to everyone in the -1 room for making me laugh every day.

Finally, I have to thanks to my family – mom, dad, aunt and sister that despite of being far away, was always available. Again, they were tireless and always prompt to provide guidance.

TABLE OF CONTENTS

LIST OF FIGURES

LIST OF TABLES

LIST OF ABBREVIATIONS

2D	Two-dimensional
3D	Three-dimensional
Akt	Protein kinase B
α-SMA	Alpha-smooth muscle actin
BSA	Bovine serum albumin
C D1	Control day 1
C D10	Control day 10
C D17	Control day 17
C D7	Control day 7
Cdc42	Cell division control protein 42 homolog
CDH1	E-cadherin gene
CDH2	N-cadherin gene
CLSM	Confocal laser scanning microscopy
DNA	Deoxyribonucleic acid
E	Elastic modulus
ECM	Extracellular matrix
EDC	1-ethyl-(dimethylaminopropyl)-carbodiimide
EMT	Epithelial-to-mesenchymal transition
EpH4	Mouse mammary epithelial cells
EthD-1	Ethidium homodimer-1
FN	Fibronectin
G	a-L-guluronic acid
G'	Storage modulus
GAPDH	Glyceraldehyde 3-phosphate dehydrogenase
GDL	Glucose delta-lactone
GTPases	Guanine nucleotide-binding proteins
HIF1α	Hypoxia-inducible factor 1-alpha
Id2	Inhibitor Of DNA Binding 2, Dominant Negative Helix-Loop-Helix
LVR	Linear viscoelastic region
MAPK	Mitogen-activated Protein Kinases
MET	Mesenchymal-epithelial transition
Mgat3	N-Acetylglucosaminyltransferase III
miR	microRNA
MMPs	Matrix metalloproteinases
NFkB	Nuclear-factor kappa B

Ocln	Occludin
ON	Overnight
Pa	Pascal
PA	Polyacrylamide
PBS	Phosphate-buffered saline
PEG	Polyethylene glycol
PFA	Paraformaldehyde
PGA	Poly(glycolic acid)
pHEMA	Poly(2-hydroxyethyl methacrylate)
PI3K	Phosphoinositide 3-kinase
PLA	Poly(lactic acid)
PLGA	Poly/lactide-co-glycolide)
Rac	Ras-related C3 botulinum toxin
RE	Reversed epithelia
RGD	Arginine-glycine-aspartic acid peptide
Rho	Ras homolog gene family
RT	Room temperature
S D1	Stiffened day 1
S D10	Stiffened day 10
S D17	Stiffened day 17
S D7	Stiffened day 7
Sulfo-NHS	N-Hydroxy-sulfosuccinimide
TBS	Tris-buffered saline
TGF-β	Tumor growth factor beta
TGF-β1	Tumor growth factor beta 1
TGFβRI	Tumor growth facto beta receptor type I
TGFβRII	Tumor growth factor beta receptor type II
Twist1	Twist-related protein 1
Vim	Vimentin
Zeb1	Zinc Finger E-Box Binding Homeobox 1
Zeb2	Zinc Finger E-Box Binding Homeobox 2
ZO-1	Zonula occludens

1. Introduction

1.1. Epithelial-to-mesenchymal transition

Epithelial-to-mesenchymal transition (EMT) plays a central role in embryonic development, wound healing and in cancer. For this reason, EMT is divided in different classes – EMT type 1 for embryonic morphogenesis and development, type 2 for inflammatory response during wound healing, tissue regeneration and organ fibrosis, and type 3 for pathophysiological circumstances [1]. The third type of EMT is being highly implicated in cancer progression [2-4]. During EMT, epithelial (E) cells progressively lose polarity and cell-cell contacts acquiring a mesenchymal (M) phenotype with increased migratory and invasive potential [4, 5] (Figure 1). EMT confers plasticity to cells, contributing to cell dispersion during development and cancer dissemination [2, 3]. In epithelial cancers, invading cells display EMT-like features such as a mesenchymal phenotype associated with expression of vimentin (M marker), and loss of epithelial E-cadherin expression, and/or detachment and movement towards the stroma [5, 6]. These cells may undergo the reverse process, mesenchymal to epithelial transition (MET), in order to grow and colonize secondary sites, forming metastasis [7]. During MET, cells regain epithelial features, such as increase of E-cadherin expression and proliferative capacity, while mesenchymal markers and transcription factors associated with EMT, namely Twist1, are downregulated [8].

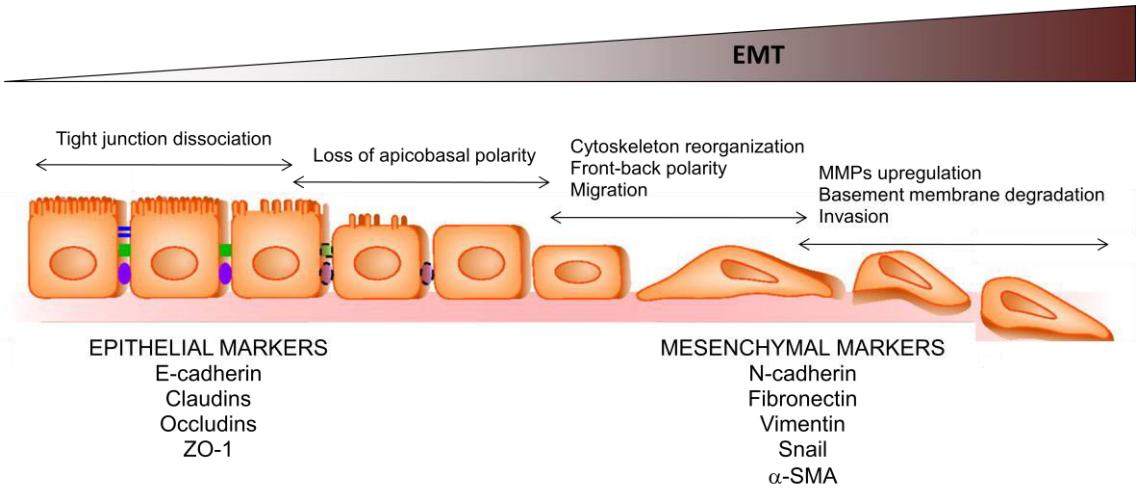

Figure 1 – Epithelial-to-mesenchymal transition (EMT) process. Epithelial cells lose cell-cell contacts and detach from the basement membrane, while acquiring mesenchymal characteristics, such as rounder aspect and capacity to invade the tissue to form metastasis (adapted from [9]).

Furthermore, due to EMT importance in cancer dissemination, this transition is acquiring a leading role in epithelial cancer studies, as genes and proteins involved in this process are being identified. Moreover, pharmaceutical compounds are being synthesized to target EMT in cancer patients [10]. Nevertheless, the clinical role of this transition is still unclear, since the majority of the studies performed on this subject were in traditional 2D models that are reductionist and offer limit insight into more physiologic behaviours, lacking the much needed proximity to animal models [11].

The molecular modifications inherent to the EMT program have been associated to key signaling pathways that may be responsible for the implementation of the cellular response to extracellular signals arising from the cell microenvironment. TGFβ1 signaling pathway is one of the best studied mechanisms of EMT induction [12, 13] and its activity is detected in cancer cells invasion [14, 15]. In physiological conditions, TGFβ1 is an essential cytokine that plays an important role in development, differentiation and homeostasis of several tissues. Moreover, it acts as a suppressor of uncontrolled proliferation and transformation [12, 13]. However, this cytokine has a double action, since its deregulation can confer an oncogenic behavior, namely in the activation of EMT in tumor cells. To initiate the TGFβ signaling pathway, TGFβ1 ligands bind to their receptors - TGFβ receptor type I and II (TGFβRI and TGFβRII) and the formation of Smad transcription factors occurs (Figure 2). These transcription factors will migrate to the cells' nucleus and assist Snail and Twist families of transcription factors [16, 17]. Besides Smad, other downstream signaling cascades will be activated upon TGFβ1 binding to its receptor, namely Rho-like GTPases, PI3K/Akt, NFkB and MAPK. All these molecules will lead to the repression of genes involved in cell polarity and adhesion, specifically RhoA and E-cadherin [18, 19]. MAPK activity can be associated with an enhanced EMT and TGFβ1-induced MAPK activity has a proliferative and anti-apoptotic effect on mesenchymal cells [20]. The proliferative action of MAPK signaling and vimentin expression, synergistically, leads to the secretion of matrix metalloproteinases (MMPs) and the reorganization of the actin cytoskeleton [21]. The cytoskeleton reorganization leads to the formation of membrane protrusions, such as filopodia, lamellipodia and invadopodia. While the first one is composed by parallel actin filaments, the other two are a branched network of actin. More specifically, invadopodia is able to degrade de ECM through MMPs secretion, namely MMP1, MMP7 and MMP9 [22]. The formation of these protrusions is also regulated by TGFβ1 signaling, since it activates small GTPases, such as Rho, Rac and Cdc42 that enhance both filopodia and lamellipodia arrangement [23]. In the TGFβ1 pathway was also observed an upregulation in N-cadherin expression, which

augments adhesion between mesenchymal cells [24]. Besides the alterations in the expression of transcription factors, microRNA expression is also modified, namely the miR200 family that repress the translation of *Zeb1* and *Zeb2* mRNAs, which are downregulated in this scenario [25].

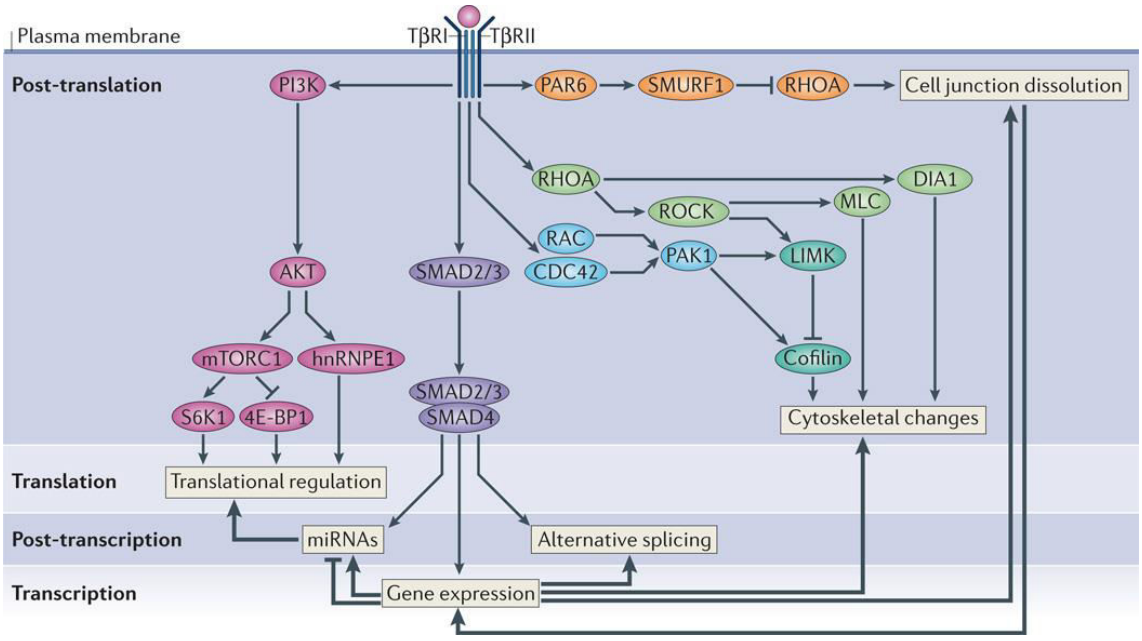

Figure 2 - Activation of TGFβ pathway by the connection with cellular membrane TGFβ receptors - TGFβRI and TGFβRII [26].

In addition to TGFβ1, other signaling pathways are closely involved in the activation of EMT. (Figure 3) Hypoxia-inducible factor (HIF) is one of those examples, since it can activate EMT transcription factors, such as Notch and β-catenin [27, 28]. HIF1-α, in particular, can induce the expression of Twist and Snail in epithelial cells and ovarian carcinoma cells [29]. Wnt signalling can also be correlated with this process, since it can inactivate glycogen synthase kinase GSK-3β, that inhibits the activation of Snail and LEF-1, thus inducing EMT and cell migration via decrease of E-cadherin and increase of mesenchymal markers [30-32]. The NFkB pathway can also be seen as an EMT regulator that will induce the transcription of Snail in carcinoma cell lines and mesothelial fibrosis [33].

Although there are different EMT inductors, the modification in the transcription program seems to result in identical outcomes. Namely, the loss of E-cadherin is always included in that alteration. In fact, the loss of E-cadherin is associated with the distinct types of EMT and has been proposed as an indicator of tumor progression and poor prognosis both in human and murine tumors [34]. For instance, it was demonstrated that the change from noninvasive to invasive pancreatic cancer in a

transgenic mouse model can be correlated with the loss of E-cadherin expression [35]. Also, it was observed that the formation of lymphogenous metastasis from human lung carcinoma was associated with reduced E-cadherin expression [36].

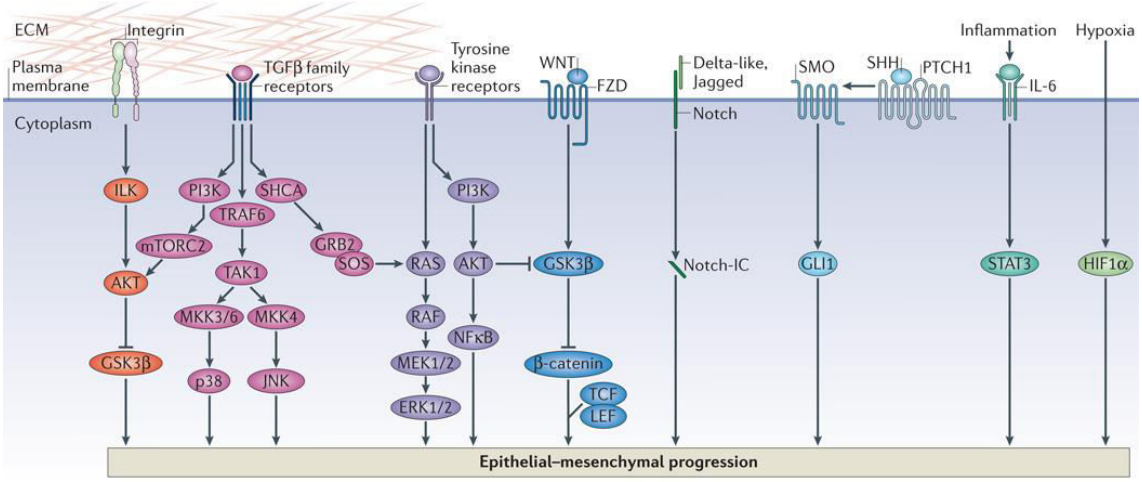

Figure 3 - Signaling pathways involved in the activation of EMT program [26].

The E-cadherin gene – *CDH1*, can bear mutations that will lead to the formation of a non-functional protein or even the absence of protein production [37] that has been related with tumor infiltration in breast cancer patients [38]. Epigenetic modifications in this gene, such as hypermethylation of the 5' CpG islands in the promotor region, leads to E-cadherin silencing. This effect has been observed in invasive breast ductal carcinoma [39], esophageal squamous cells carcinoma [40] and gastric cancer [41]. Indeed, in gastric cancers the hypermethylation of *CDH1* was found to be correlated with cancer aggressiveness and metastasis [42]. Snail, Slug and ZEB1/2 can bind directly to the E-box repressive elements in the promoter of *CDH1*, inhibiting its transcription [43]. Snail-induced EMT could enhanced metastasis formation in both human and mouse malignant melanoma [36]. Post-transcriptional modification of E-cadherin can also occur, normally through phosphorylation or glycosylation [44, 45]. The loss of E-cadherin is associated with an increase of N-cadherin [46], which is a mesenchymal marker.

1.1.1. Role of matrix mechanical properties in EMT

Cancer progression (initiation, growth, invasion and metastasis) occurs through direct contact and/or via paracrine signaling between malignant cells and the surrounding tumor stromal cells. The tumor microenvironment is comprised by biochemical and

biomemechanical cues, as well as of a variety of cell types, such as fibroblasts, immune cells, vascular endothelial cells, pericytes and bone-marrow-derived cells, embedded in the ECM [47]. Therefore, EMT may be regulated not only by TGFβ1 but also by mechanical forces of the ECM. As demonstrated by Leight and colleagues, matrix rigidity regulates a switch between TGβ1-induced apoptosis and EMT [48]. To assess this, normal murine mammary gland cells (NMuMG) were cultured on polyacrylamide (PA) hydrogels with varying rigidity (0.4 to 60 kPa) and treated with TGFβ1 (0.1 to 1 ng/ml) [48]. They observed that the culture on different stiffness levels led to morphological differences, since in rigid substrates (E>14 kPa) cells were cuboidal, while in compliant matrices (E<1 kPa) they were rounded and formed spherical clusters. Treatment with TGFβ1 in rigid matrices led to elongated cell morphology and scattering of cells, both characteristic features of EMT. These results were further confirmed by delocalization of E-cadherin and upregulation of mesenchymal markers, such as N-cadherin, α-SMA and Snail. Noteworthy, this TGFβ1 action was higher in substrates from 1 to 8 kPa, which is similar to the stiffness of an excised tumor tissue (~4 kPa [49]). On softer gels, TGFβ1 induced apoptosis. Overall, these results demonstrated that matrix rigidity can regulate the cellular response to TGFβ1. In another study, using alveolar epithelial cells (RLE-6TN) cultured on PA hydrogels (from 2 to 32 kPa) with fibronectin conjugated with different recombinant variants of the RGD sequence, Markowski *et al.* also concluded that TGFβ1 (up to 0.1 ng/mL) induced EMT only on stiff substrates (32 kPa) [50]. In fact, cells in 2 kPa hydrogels maintained an epithelial phenotype with prominent E-cadherin and low α-SMA staining. However, at 32 kPa, E-cadherin levels decreased while α-SMA increased. Cytoskeleton rearrangements and stress fiber formation, which are markers of a transition to a mesenchymal phenotype, were significantly increased in cells cultured in stiffer hydrogels [50]. In the work of Gill and colleagues they used a metastable cell line (344SQ) with KRas and p53 mutations cultured within poly(ethylene glycol) (PEG) matrices (from 21 to 55 kPa) modified with bioactive peptides [51]. They observed that independent of matrix composition, exposure to TGFβ1 (5ng/mL) induced a loss of epithelia morphologic features, shift in expression of EMT marker genes (decrease of epithelial markers, such as *CDH1*), an increase in mesenchymal ones (*CDH2*, *Vim* e *Zeb1*) and decrease in miR-200 levels. Noteworthy, the matrix stiffness range analyzed in this study was higher than the range evaluated in previous studies. This could explain why the authors observed EMT induction in all PEG formulations.

Recently, Wei *et al.* developed a collagen-coated PA hydrogel with rigidity ranging from 150 Pa to 5700 Pa in a 3D matrigel overlay culture system, with MCF10A and EpH4Ras cells [52]. They demonstrated that increasing matrix stiffness in the tumor microenvironment directly activates EMT, tumour invasion and metastasis through EMT-inducing transcription factor TWIST1. At lower elastic modulus, both cell types developed polarized ductal acini surrounded by intact basement membrane; however, in stiffer matrices, a partial EMT phenotype was encountered with destabilized basement membrane. A silencing of TWIST1 was performed in both cells, resulting in the prevention of an invasive phenotype at 5700 Pa, which was maintained even in the presence of TGFβ1 (5ng/mL). In the model of TWIST1 knockdown, mRNA levels of Snai2, *Zeb1* and *Zeb2* were reduced, leading to the conclusion that TWIST1 has a key role in the EMT gene response. Moreover, it was observed that TWIST1 has a nuclear localization in stiffer matrices, while in softer ones, this molecule is cytoplasmic and binds to G3BP2. High matrix stiffness promotes nuclear translocation of TWIST1 by releasing TWIST1 from its cytoplasmic binding partner G3BP2. Loss of G3BP2 and rising of matrix stiffness synergistically resulted in destabilization of basement membrane, downregulation of E-cadherin and higher expression of vimentin. In this work, TWIST1 was found to be a mechanomediator that enhances EMT at higher rigidity of the matrix.

In fact, the ECM mechanical properties do play a crucial role on EMT induction and in the extent of the transition, leading to invasiveness and poor prognosis. Despite that the studies here presented used different materials to mimic the ECM and distinct ranges of stiffness, it seems clear that high matrix stiffness promote an EMT phenotype. Nevertheless, as this view of ECM's mechanical role on cancer progression is very recent, more studies need to be performed to address this question.

1.1.2. *In vitro* platforms to study EMT: 2D vs 3D systems

2D systems have been widely used in cancer research due to their easy manipulation, reproducibility and the existence of a wide range of biochemical analysis readily adaptable to this type of platform. However, 2D analysis lack essential features present in physiological and pathological natural microenvironments. For example, one of the limitations of 2D cell culture is that cells form a monolayer of polarized cells with only one side of their surface area attached to the substrate and the remaining surface in contact with culture medium. This type of morphology can greatly limit tissue-specific functions of the cellular type under study [53]. Thus, traditional 2D fail to recapitulate key architectural features of the tumor microenvironment.

Differences observed between 2D and 3D cell culture models of EMT have been described in a few studies. For example, Maschler *et al.* found that EpH4 cells (transformed with oncogenic Ha-Ras), when stimulated with TGFβ1 (8ng/mL) to induce EMT, were able to secrete tenascin-C, which is an ECM protein known to be overexpressed in breast cancer. However, this phenomenon only occurred in 3D collagen cell culture, since cells cultured in 2D had no significant differences in tenascin-C levels [54]. In another study, Loessner *et al.* compared the interactions that occur between cells and the ECM in 2D vs 3D culture using two human cancer cell lines, namely epithelial ovarian cancer and serous adenocarcinoma cell lines. In 3D, the cells had higher proliferation rate comparing to 2D, which was dependent on cell-integrin connection and on the ability to remodel the matrix [55]. Using a 3D substrate of chitosan-hyaluronan to promote tumor spheroid formation, Huang and colleagues studied EMT markers in non-small cell lung cancer cells (NSCLC) and compared to these cells cultured in 2D. The EMT markers, such as N-cadherin, vimentin, CD44, among others, were increased in 3D culture. Also, cells in 3D had increased invasion behavior, seen by the higher expression of matrix metalloproteinases, namely MMP2 and MMP9, and presented higher multidrug resistance [56].

Another study on EMT with A431 (human squamous cell carcinoma) showed significant differences between 2D and 3D cell culture [57]. Here, 3D culture was performed with a radial flow type bioreactor that contained a high pore matrix of hydroxyapatite beads. First, the authors assessed the expression of common transcription repressors of E-cadherin gene after the treatment with TGFβ1 (1ng/mL) in both 2D and 3D. Slug, Goosecoid and LEF1 were up-regulated in the 3D culture, as well as HEY1 gene, which is a target of Notch and HMGA2 that is a regulator of TGFβ1/Smad signaling. All these factors seemed to be decreasing the levels of E-cadherin, in a 3D-dependent manner. Besides E-cadherin expression, both mRNA and protein levels of β-catenin were higher in 3D culture and the mesenchymal markers, such as vimentin and fibronectin were also increased in 3D culture. In fact, these mesenchymal markers could not be detected in 2D cell culture. A431 cells in 3D seemed to be losing their epithelial polarity when stimulated with 1ng/mL of TGFβ1, which was proved by the downregulation of tight junctional proteins, namely occludin, claudin and ZO-1. Integrin subunits, seen by both mRNA and protein levels, were also upregulated in 3D cell culture, namely integrin α5 and integrin αv, both known as fibronectin receptor and tenascin receptor, only for the last one. Interestingly, the authors also performed similar studies in nude mice xenotransplanted with A431 tumor tissues. The results were

identical to the ones found in 3D culture, which again highlights the importance of 3D cell culture and its ability to better mimic the *in vivo* environment.

The paradigm shift from 2D to 3D culture is underway and progressing rapidly, being currently recognized that adding the 3rd dimension to a cell's environment creates significant differences in cellular characteristics and function [58]. M Bissel's team elegantly demonstrated the relevance of using 3D systems to investigate cancer mechanisms, by creating a prototypical model of the mammary gland acinus, where TGFβ1-induced EMT occurred [59]. 3D models where cells are completely surrounded by a supportive 3D matrix, i.e. hydrogel-based entrapment systems, are the most relevant systems for modulating cell-matrix interaction. In this type of systems, a crosstalk between chemical, physical and mechanical signaling will occur, modulating cellular responses (Figure 4).

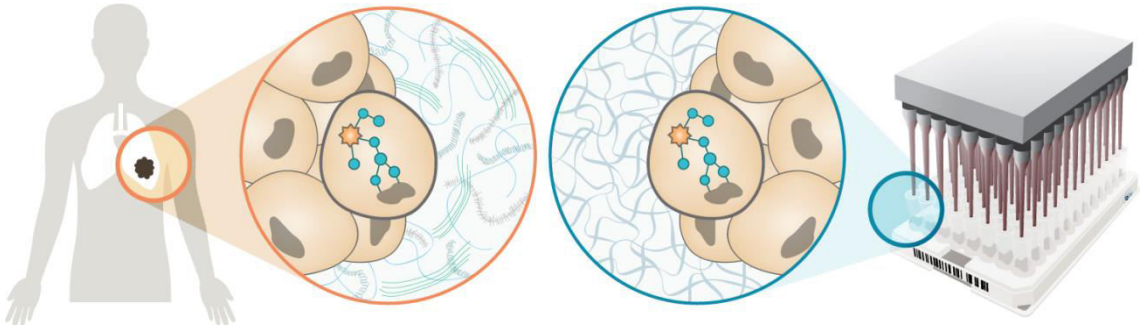

Figure 4 – 3D cell culture recapitulates the *in vivo* microenvironment. In 3D, cells are entrapped, surrounded by the ECM, allowing for the inter-connection between chemical, physical and mechanical signaling (adapted from [60]).

1.2. Hydrogels as attractive ECM mimics

Hydrogels are one of the most used materials to mimic ECM, mainly because they have similar structural, viscoelastic and diffusive transport properties, as well as high biocompatibility [61, 62]. Hydrogels are mainly composed of water that fills in between network crosslinks and the high amount of water in its composition is responsible for their high permeability. Physiologically in the ECM, diffusive transport is maintained by the pores that exist in between cells. To replicate this property, hydrogels can be performed with controlled crosslinking density [62].

Hydrogels can be produced from both natural and synthetic sources and their applications have been consistently increased, going from regenerative medicine, to drug delivery systems and cancer research.

Hydrogels based on ECM derived protein gels such as collagen or Matrigel are commonly used to produce such 3D systems, but generally present high batch-to-batch

variability, intrinsic bioactivity and poorly tunable biochemical/biomechanical properties [63]. More recently, biomaterial-based platforms traditionally associated with tissue engineering approaches have been translated into cancer research creating improved models to study tumor biology [51, 63-65]. In this context, other types of systems have also been explored, namely polysaccharide-based hydrogels such as chitosan and alginate, and synthetic materials, like polylactic acid (PLA), polyglycolic acid (PGA), polylactic-co-glycolic acid (PLGA) and polyethylene glycol (PEG), among others. Polysaccharide-based and synthetic materials present some advantages over protein-based hydrogels, such as higher batch-to-batch uniformity and more stable physical and chemical composition that can be tuned. However, synthetic hydrogels do not present intrinsic bioactivity, being unable to promote specific cell-matrix interactions. Nevertheless, hybrid hydrogels incorporating bioactive moieties can be prepared. For example, cell adhesive peptides, like the well known Arginine-Glycine-Aspartic acid (RGD), can be added to otherwise inert substrate to promote cell-matrix adhesion. Many other components can be added, such as proteins (for instance, growth factors) and also peptides sensible to matrix-proteases (MMPs) for promoting cell-driven remodeling processes [53]. A summary of different advantages and disadvantages of natural vs synthetic hydrogels is described in Table 1.

Table 1 - Classes of materials used in 3D cell culture – natural (protein or polysaccharide-based) and synthetic. Advantages and disadvantages of the use of different materials are present in this table (adapted from [63]).

	Naturallly derived matrices	Synthetic matrices
Examples for 3D culture	Collagen and Matrigel (protein-based), Alginate and Chitosan (polysaccharide-based) Permit 3D culture in physiological conditions with high viability	PA (toxic to 3D culture), PLA, PLG and PLGA (require processing steps) and PEG (compatible with 3D culture)
Bioactivity	Baseline bioactivity with ample ligands for cell adhesion and signaling; difficult to isolate specific bioactive factor for experimental study	Requires passive protein absorption (PLA, PLG and PLGA) or extra engineering (PEG); greater control over bioactivity with less experimental confounding
Mechanical properties	Tunable via additional crosslinking; generally alters ligand density; limited to low-range elasticities	Tunable with minimal/no bioactivity change; broad range of physiological elasticities
Matrix degradation	Cell-mediated matrix remodeling; difficult to control	Predictable degradation of synthetic material; requires modification for cell-mediated degradation
Growth factor contamination	Difficult to completely remove (protein-based)	None with synthetics

PA, polyacrylamide; PLA, poly(lactic acid); PLG, poly(lactic-co-glycolic acid); PEG, poly(ethylene glycol).

1.2.1 Alginate hydrogels as substrates for 3D cell culture

Alginate is a natural polymer extracted from brown algae. It is an unbranched polyssacharide composed by 1,4-linked β-D-mannuronic acid (M) and α-L-guluronic acid (G) residues covalently linked that vary in composition and sequence (Figure 5) [66]. They can be arranged in different types of sequences, namely MM-blocks, GG-blocks and MG-blocks [67]. Alginate is found in the algae intracellular matrix as a mixed salt of various cations found in sea water such as Mg^{2+}, Ca^{2+}, Sr^{2+}, Ba^{2+}, and Na^{+}; however it is mainly present as a Ca^{2+}-crosslinked gel [66].

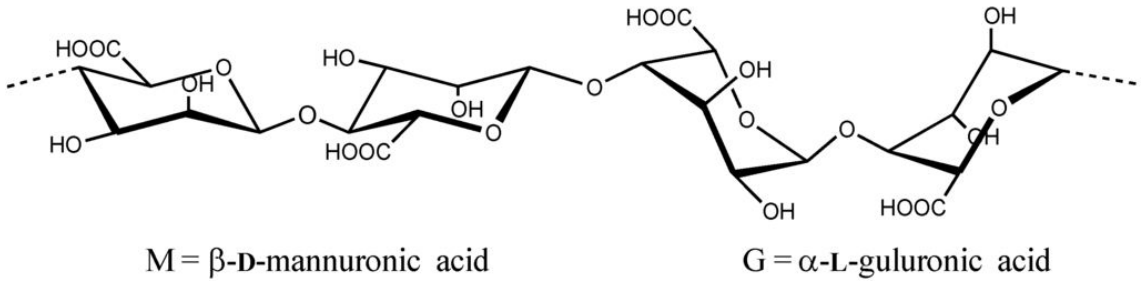

Figure 5 - Alginate structure and residues β-D-mannuronic acid (M) and α-L-guluronic acid (G) [68].

Alginate is able to form hydrogels under mild conditions and at physiological temperature and pH [69]. Another advantage of alginate hydrogels is that their mechanical properties can be easily tuned, so that it is possible to mimic different tissue stiffness levels. To achieve different stiffness values, the molecular weight, concentration or the degree of crosslinking can be altered or chemical modifications can be performed [70]. The compression modulus of alginate hydrogels can range from 1 to 1000 kPa and the shear modulus from 0.02 to 40 kPa [71]. The major disadvantages of alginate are the low biodegradation rate and the lack of patterns for cell recognition. However, both can be overcome by chemical and biochemical modifications [72-78].

Alginate has high affinity to a variety of divalent cations, such as Ca^{2+}, Sr^{2+} and Ba^{2+}, which crosslink the hydrogel network, a mechanism known as ionic crosslinking, due to their affinity to GG blocks [67]. The crosslink with cations mainly occurs between negatively-charged carboxylic moieties of adjacent alginate chains [79] (Figure 6). This affinity decreases in the order $Pb^{2+} > Cu^{2+} > Cd^{2+} > Ba^{2+} > Sr^{2+} > Ca^{2+} > Co^{2+}$, Ni^{2+}, $Zn^{2+} > Mn^{2+}$ [80, 81].

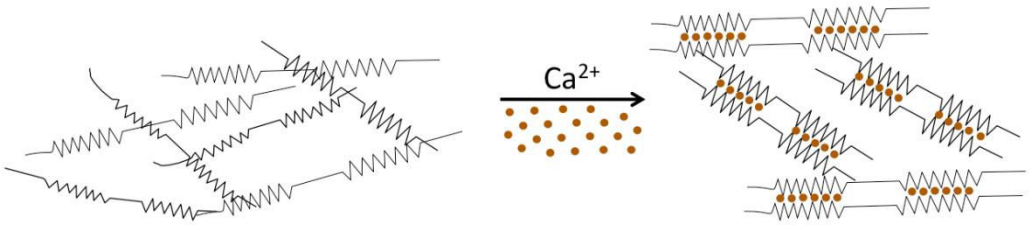

Figure 6 - Alginate ionic crosslinking performed by calcium ions (Ca^{2+}) [69].

To form hydrogels, calcium ions are the most commonly used. Gelation can occur under external and internal conditions (*in situ*). The first one uses soluble salts such as calcium chloride ($CaCl_2$), but this process, although it happens almost instantly, can lead to different crosslinking densities and concentration gradients across the hydrogel [82, 83]. Internal gelation with low solubility divalent cation salts, like calcium carbonate ($CaCO_3$) or calcium sulfate ($CaSO_4$), aims to diminish the gelation rate so that the process can be more easily controlled, leading to formation of homogenous gels [82]. Even though Ca^{2+} is an essential ion for cells, several studies used this ion for alginate crosslinking in tissue engineering constructs for different cell types; and all of them reached the conclusion that Ca^{2+} is well endured by cells that are in contact with crosslinking and uncrosslinking activities in alginate [84-88]. However, due to the intrinsic role that calcium ions play in cell-cell and cell-matrix interactions [89, 90] alternative crosslinking agents should be explored as possible alternatives. For instance, Ba^{2+} is also being widely used [91-95] and Ba^{2+}-alginate gels are stronger than Ca^{2+}-alginate ones [96]. However, it has been reported that barium may inhibit the K^+ channels, so Ba^{2+} concentration should be kept to a minimum [97]. Strontium ions appear as a more interesting alternative, as they are considered to be non-toxic and form more stable hydrogels than calcium crosslinked alginate [97].

Morch *et al.* performed a study to characterize different properties of alginate gels with calcium, barium or strontium [97]. High-G Ca^{2+}-alginate beads were larger than beads of high-M alginate and, when in the presence of barium or strontium, it was observed an initial size increase. The swelling of high-G alginate beads with barium and strontium was reduced. For high-M alginate, no reduction on swelling was observed after exchanging Ca^{2+} with Sr^{2+} or Ba^{2+}. The hydrogels' elastic modulus was determined in alginate gel cylinders by small deformation compression. High-G alginate gels were stronger than the high-M alginate for all the ionic crosslinkers tested, which is concordant with other studies [79]. For high-G alginate, even very low concentrations of strontium or barium increased the gel strength dramatically.

Strontium could increase the gel strength, even more than with calcium at the same concentration; however, to a lesser extent than barium [97].

In ionic alginate hydrogels, increasing the concentration of crosslink ions and/or the time of crosslinking may reinforce the crosslinking degree. On the other hand, the process can be reverted since crosslinking ions may be displaced by chelators (such as phosphate and citrate) and non-gelling cations (such as sodium and magnesium ions [97]), which can lead to swelling, increased pore size and ultimately gel destabilization and disintegration [98, 99]. These two properties allow the mechanical aspect of alginate-based hydrogels to be tuned 'on demand', as it is possible to submit the hydrogels to crosslinking/uncrosslinking cycles For example, Gillette et al [100] developed a dynamically switchable two-component collagen-alginate 3D matrix, where collagen acted as structural element, and alginate could be submitted to crosslinking/uncrosslinking cycles. Using $CaCl_2$ as a crosslinker and sodium citrate (calcium chelator) as an uncrosslinking agent, the authors were able to change hydrogel mechanical properties *in situ*. Cells entrapped within these hydrogels were unable to spread or migrate when the matrix was in the uncrosslinked state, but not in the crosslinked state. In the former case, when uncrosslinked matrices were re-crosslinked, cells remained spread but were unable to move.

1.3. Aim of the thesis: developing upgraded 3D *in vitro* models of EMT

To explore the phenotypic and transcriptional switching of cells during EMT, the Expression Regulation in Cancer group at IPATIMUP established an *in vitro* 2D model of TGFβ1-induced EMT and its reversion [45, 101]. TGFβ1 supply to the near-normal E cell line EpH4 efficiently generated M-like cells, and its removal resulted in the re-acquisition of an epithelial-like phenotype. The later cellular state, which was named reversed epithelia (RE cells), is characterized by the co-existence of several and heterogeneous cellular populations with regard to the expression of E-cadherin (E marker) or fibronectin (M marker) [101]. In that 2D model, it was also demonstrated that RE cells, generated through MET, together with heterogeneity display increased self-renewal potential and *in vivo* tumourigenesis ability [101]. RE cells, unlike E and M, possibly reproduce tumor heterogeneity often described in primary and metastatic clinical samples [102, 103]. Still, as already discussed, traditional 2D models are reductionist and may offer limited insight into more physiologic behaviors, as they fail to recapitulate key architectural features of the tumor microenvironment.

Therefore, in a recent work in collaboration with INEB, the established 2D model evolved towards a new 3D *in vitro* model [104], by combining the inducible epithelial

cell line (EpH4) with a bioengineered ECM-like matrix with tunable properties, to explore the inter-conversion between E and M states during EMT/MET. The selected 3D matrix, composed of an optimized soft alginate hydrogel functionalized with cell adhesive RGD peptides [73, 77], supported epithelial morphogenesis and allowed TGFβ1-induced generation of cells with mesenchymal-like and intermediate phenotypes, providing a useful tool to unravel cellular alterations associated with EMT/MET [104].

The main aim of this thesis was to further up-grade this 3D model, by optimizing a method for dynamically switching matrix viscoelastic properties, *in situ*, which will allow an improved understanding of the impact of the ECM biomechanics in EMT. This type of studies is expected to improve current knowledge on cancer progression and dissemination processes, and may pave the way for the identification of putative targets for more effective anti-cancer therapies.

2. Materials and Methods

2.1. Synthesis and characterization of RGD-alginate

Ultrapure sodium alginate (PRONOVA UP LVG, Novamatrix, FMC Biopolymers) with a molecular weight of 150 kDa and a high content of guluronic acid (~70%) was covalent grafted with the cell-adhesion peptide (glycine)4-arginine-glycine-aspartic acid-serine-proline (hereafter abbreviated as RGD) using aqueous carbodiimide chemistry as previously described [105]. Briefly, alginate solutions (1 wt.%) in MES buffer (0.1 M MES, 0.3 M NaCl, pH 6.5) were prepared and stirred overnight (ON) at room temperature (RT). N-Hydroxy-sulfosuccinimide (Sulfo-NHS, Pierce) and 1-ethyl-(dimethylaminopropyl)-carbodiimide (EDC, Sigma, 27.4 mg per g of alginate) were sequentially added at a molar ratio of 1:2, followed by 100 mg of RGD peptide (Genscript) per g of alginate. After stirring for 20 h at RT, the reaction was quenched with hydroxylamine (Sigma) and the solution was dialyzed against deionized water for 3 days (MWCO 3500). After purification with charcoal, RGD-alginate was lyophilized and stored at -20ºC until further use. The reaction yield was calculated using the BCA Protein Assay (Pierce), as previously described in Ref [74].

2.2. Preparation of RGD-alginate hydrogel matrices

In situ forming alginate hydrogel matrices were prepared by internal gelation as described previously [73, 74, 77]. Hydrogel precursor solution was prepared at 1 wt.% sodium alginate in 0.9 wt.% NaCl, with 200 µM RGD, a density comparable to that present in commonly used ECM-derived biological matrices [106]. The solution was sterile-filtered (0.22 µm) and mixed with an aqueous suspension of sterile $CaCO_3$ (Fluka) at a $CaCO_3$/COOH molar ratio of 1.6 [107]. Then, a fresh sterile solution of glucone delta-lactone (GDL, Sigma) was added to trigger gelation. The $CaCO_3$/GDL molar ratio was set at 0.125, and the gelation time was 30 to 45 min.

2.3. *In situ* stiffening and softening of RGD-alginate hydrogel matrices

For stiffening, acellular or cell-laden (prepared as described in the next section) alginate hydrogels were transferred to 8 µm transwells (eppendorf) and placed in a solution of $CaCl_2$ (0.1 M or 50 mM) or $SrCl_2$ (50 mM or 25 mM) for different periods of time. For softening, hydrogels in transwells were placed in sodium-citrate (50 mM, 25

mM or 12.5 mM) for different periods of time. Two cycles were carried out where the same hydrogels were stiffened (with $CaCl_2$ or $SrCl_2$) and then softened (with sodium-citrate) and vice-versa. After immersion on these solutions, the transwell was moved to a well with culture medium for 30 minutes to reach equilibrium.

Rheological measurements were carried out using a Kinexus Pro rheometer (Malvern). Hydrogel discs without cells were analyzed at day 0 (after swelling to equilibrium in culture media for 1 h) under standard culture conditions. For cellular hydrogels, discs were only analysed after one day of stiffening. To guarantee the dimensional homogeneity of the samples, 4 mm cylinders were punched from the original ones immediately before analysis. All samples were assayed using a plate-and-plate geometry (4 mm diameter, sandblasted surfaces) and were compressed to 30% of their original thickness to avoid slippage. A solvent trap was used to minimize sample drying. All measurements were performed at 37 ºC (Peltier system). Stress sweeps (0.1 Hz) were first performed to determine the LVR. Frequency sweeps (0.01–2 Hz) were then performed within the LVR. The values of the shear storage modulus (G') were obtained at a frequency of 0.1 Hz. Samples were analyzed at least in triplicate.

To optimize acellular alginate hydrogels rheological properties, unmodified alginate was used and crosslinked with either $CaCO_3$ or $SrCO_3$. For the first case, hydrogels were prepared as described above and for the $SrCO_3$-based hydrogels, the $SrCO_3$/GDL ratio was also set at 0.125, but the concentration of $SrCO_3$ used was half of the $CaCO_3$.

2.4. 3D culture of EpH4 cells in RGD-alginate matrices

For cell entrapment, EpH4 cells [108] (5 x 10^6 cells/mL) were combined with RGD-alginate solution and crosslinking agents and the mixture was pipetted (20 µL) onto Teflon plates separated by 750 µm-height spacers. To quantify spheroid formation during epithelial morphogenesis discs with 8 µL and 250 µm height were made. After gelation, 3D matrices were transferred to pHEMA-treated 24-well culture plates. Thereafter, fresh medium was added and renewed after 1 h. 3D culture of EpH4 (classified as E for epithelial) were maintained in DMEM/F-12 with glutamax (Gibco) supplemented with 5% v/v FBS (Biowest), 1% v/v penicilin/streptomycin (Gibco) and 5 µg/mL insulin solution human (Sigma).

2.5. Viability, proliferation and metabolic activity in 3D

Cell viability was evaluated using the Live/Dead assay. Cell-laden matrices were washed three times with DMEM/F-12 without phenol red (Gibco), then incubated (45 min, 37 ºC in the dark) with calcein AM (1 µM, live cells) and ethidium homodimer-1 (EthD-1, 2.5 µM, dead cells) and washed again. Samples were imaged by confocal laser scanning microscopy (CLSM, Leica SP2 AOBS SE).

Cell proliferation was assessed by Ki-67 immunostaining. EpH4-laden hydrogels were fixed with 4 wt.% paraformaldehyde (PFA, Sigma) in TBS-Ca (TBS with 7.5 mM $CaCl_2$) for 20 min, permeabilized for 5 min with 0.2% v/v Triton X-100/TBS-Ca, and then incubated for 1 h in 1 wt.% bovine serum albumin (BSA) in TBS-Ca to block unspecific binding. Finally, samples were incubated with goat anti-rabbit secondary antibody Alexa Fluor 488 (Molecular Probes, Invitrogen, 1:1000, 1 h at RT) and nuclei were counterstained with DAPI.

Cell metabolic activity was assessed using the resazurin assay. Cell-laden matrices were incubated with 20%v/v of the stock resazurin solution (0.1 mg/mL, Sigma) in medium for 2 h at 37ºC. The supernatant was then transferred to a 96-well plate black with clear bottom (Greiner) and fluorescence measurements were carried out using a microplate reader (Biotek Synergy MX) with Ex/Em at 530/590 nm. For each condition n=3 replicates were analyzed from 3 different biological replicas.

2.6. Analysis and quantification of spheroids formation

For analysis of spheroids formation, EpH4 cells were pre-labeled with CellTracker Green CMFDA (Molecular Probes) at 15 µM for 30 min, and then entrapped within alginate matrices as described. Whole-mounted samples with fluorescence-labeled cells within alginate matrices were imaged by CLSM at different time points (days 1, 7 and 14). For quantifications of spheroids number and size during epithelial morphogenesis, EpH4-laden hydrogels were fixed, permeabilized and blocked as described above. F-actin filaments were stained with Alexa Fluor 488 phalloidin (Invitrogen, 1:40 in 1 wt.% BSA/TBS-Ca, 1 h at RT) and nuclei were counterstained with DAPI. Samples were analysed by CLSM. The scanned Z-series were projected onto a single plane and spheroid diameter and number was assessed with Fiji. Three independent gels were analyzed for each condition and 1316 spheroids images were analyzed overall.

For the quantification of spheroids diameter in the case of matrix stiffening versus control samples, samples were also fixed, permeabilized and blocked; however, only

DAPI staining was performed. The results were visualized by CLSM and analysed in Fiji, as described above. In this case, only one hydrogel was considered per condition.

2.7. Phenotypic analysis by immunofluorescence

EpH4-laden matrices were fixed, permeabilized and blocked as described in previous section. Subsequently, samples were incubated with the following primary antibodies: rabbit anti-E-cadherin (Cell Signalling, 1:100, 2 hours at RT) and rabbit anti-Vimentin (GenScript, 1:100, overnight at 4ºC). Finally, samples were incubated with goat anti-rabbit secondary antibody Alexa Fluor 594 (for E-cadherin) and 488 (for vimentin) (Molecular Probes, Invitrogen, 1:1000, 1 h at RT) and nuclei were counterstained with DAPI.

2.8. mRNA expression by qRT-PCR

RNA was extracted from EpH4-laden matrices using the Quick-RNA MiniPrep (Zymo Research), as recommended by the manufacturer. Subsequently, 1000 ng of total RNA were reversed transcribed to single stranded cDNA using Superscript First-strand synthesis and random hexamer primers (Invitrogen). Quantitative Real-Time PCR (qRT-PCR) was carried out using source RNA from one biological replica for the target genes *CDH1*, *Ocln*, *CDH2*, *Zeb2*, *Mgat3*, *Id2* and for endogenous control GAPDH using as probe sets Mm00486909, Mm.PT.47.16166845, Mm00483212_m1, Mm.PT.47.13169136, Mm00447798_s1, Mm00711781_m1, 4352932 (Applied Biosystems and Integrated DNA Technologies) respectively. Samples were run in triplicates in the ABI Prism 7000 Sequence Detection System and data was analysed by the comparative 2(-ΔΔCT) method [109].

2.9. Matrix metalloproteinases (MMPs) secretion by gelatin zymography

To detect secretion of MMPs (MMP2 and MMP9) by 3D cultured cells, cell culture supernatants were analyzed by gelatin-zymography from 1 biological replica. After 72 h after contact with the discs, conditioned media were collected, centrifuged to remove cell debris and loaded into gelatin-SDS polyacrylamide gels. Sample volumes were adjusted to yield equivalent total cell protein contents, which were quantified by the BCA Protein Assay (Pierce) in lysates of cells recovered from the hydrogels [74]. The gel was run in 1x Tris-Glycine SDS running buffer at 60 V (Mini Protean Tetra Cell

system, BioRad). After electrophoresis, gels were washed twice and subsequently incubated in MMP substrate buffer for 16 h at 37ºC. Afterwards, gels were washed and stained with Coomassie Brilliant Blue R-250 (Sigma). MMPs proteolytic activity was visualized as the presence of clear bands against a blue background of Coomassie Blue-stained gelatin substrate. Thereafter, the gel was washed with distilled water, scanned using the GS-800 Calibrated Densiometer (Bio-Rad) and MMPs activity was estimated by densitometric analysis (QuantityOne, Bio-rad).

2.10. Statistical analyses

Statistical analyses were performed using GraphPad Prism 6.0 software version 6.0f. The non-parametric Mann–Whitney test was used to compare two groups. To compare spheroid diameter and number, Unpaired t test was used. Results for all analysis with ‘p’ value less than 0.05 were considered to indicate statistically significant differences.

3. Results and Discussion

3.1. Stiffness of RGD-alginate matrices can be dynamically switched *in situ*

3.1.1. Stiffening and softening of acellular hydrogels

The storage modules (G') of acellular RGD-alginate hydrogels crosslinked with $CaCO_3$ was around 700-800 Pa, in average. To induce stiffening (Figure 7), hydrogels were placed either in contact with 50 mM $CaCl_2$, at previously optimized concentration (data not shown), for different periods of time (Figure 8A). Only 3 min of contact between the hydrogels and the solution were enough to significantly increase the storage modulus of the 3D matrices up to 4431±133.60 Pa, which was not further altered upon treatment for the longer time periods analyzed (5 and 15 min). This was probably because the diffusion of calcium ions into the network was very fast, and calcium-binding sites in alginate chains became rapidly saturated. A Student's t-test was conducted and there were significant differences between the control and all the hydrogels submitted to $CaCl_2$ solution ($p<0.0001$). Since 3 min were enough to observe a significant difference, attaining a level of stiffness comparable to that of tumor tissues [49] this time period was chosen for the subsequent studies.

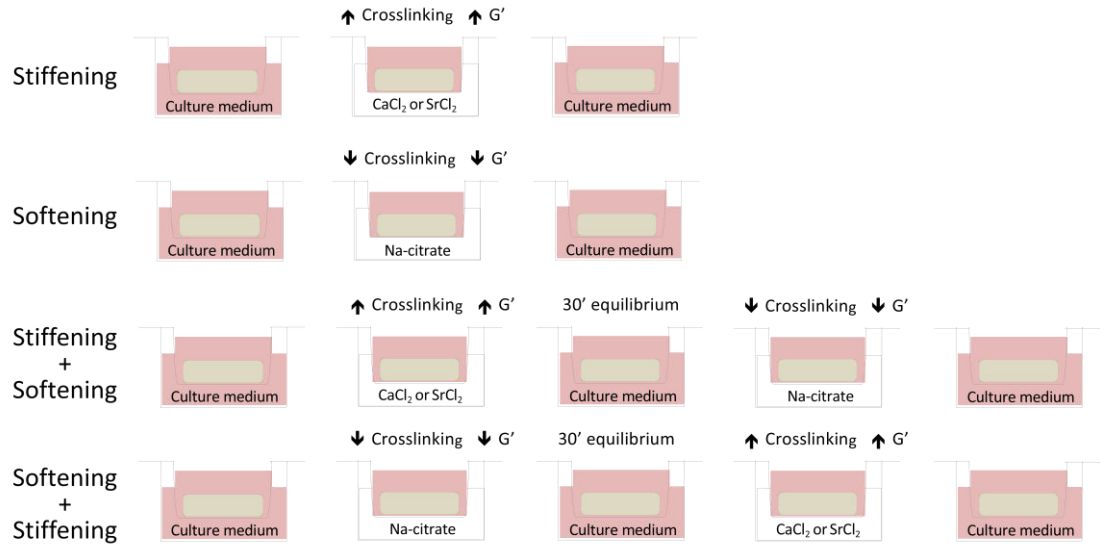

Figure 7 - Schematic representation of the process used for stiffening and/or softening acellular hydrogels.

On the other hand, to induce softening (Figure 7), hydrogels were placed in 25 mM Na-citrate for 3 minutes (also an optimized condition, data not shown), which decreased their storage modulus (324.4±126.30 Pa) to levels lower than those of control hydrogels (800 Pa, $p<0.0001$, Figure 8B). This behavior was expected, since Na-citrate

acts as a calcium chelator, sequestering the crosslinking calcium ions from the hydrogel network, thus diminishing its integrity and, consequently, the overall storage modulus.

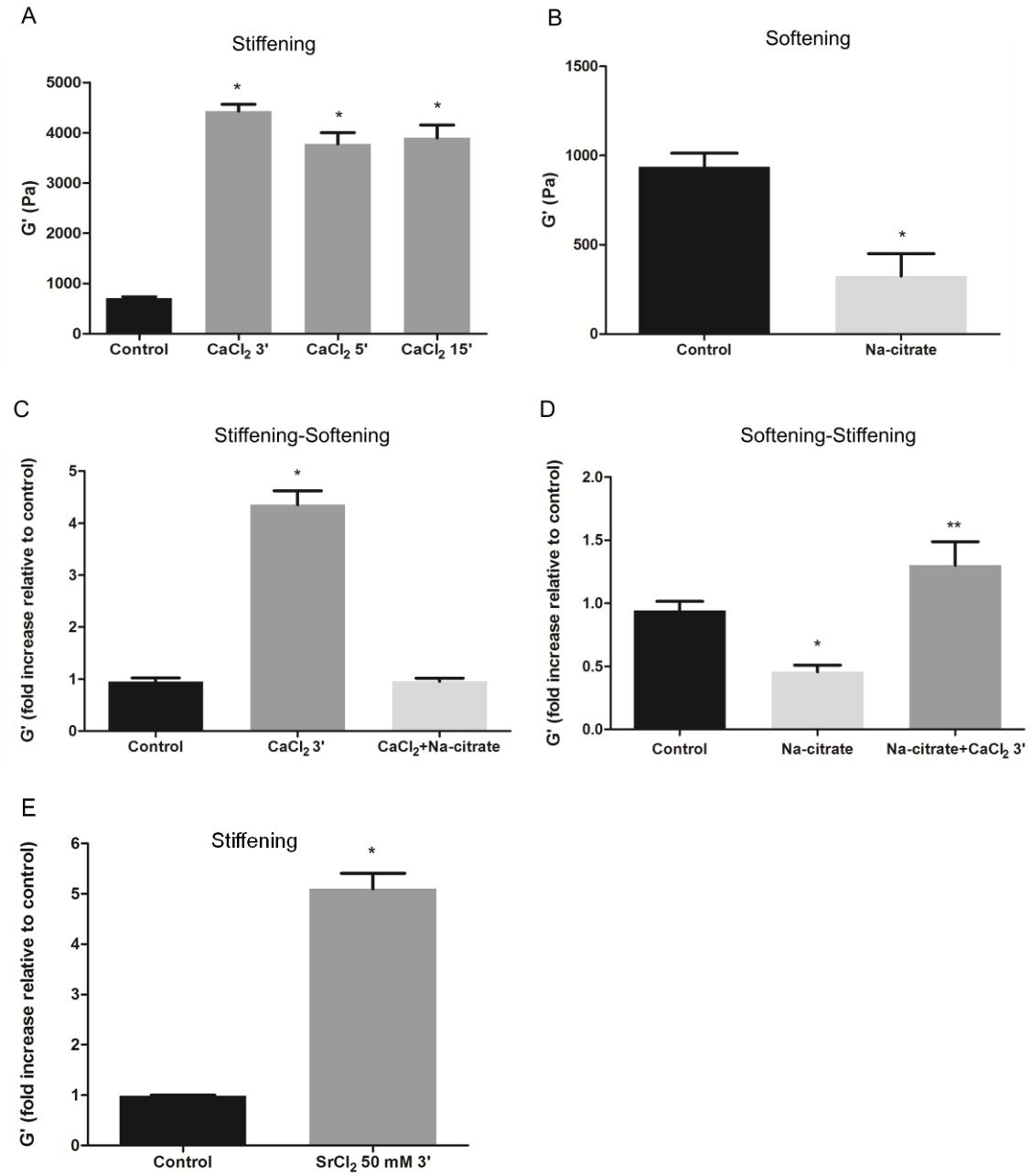

Figure 8 - Viscoelastic properties (G'-storage modulus, Pa) of Ca-alginate hydrogels submitted to stiffening and/or softening processes. (A) Hydrogels stiffening with 50 mM $CaCl_2$ for 3, 5 and 15 min. Data is presented as mean ± stdev (n=3). Significant differences were found in stiffened hydrogels (for all time periods) as compared to control (*p<0.0001). B) Hydrogels softening with 25 mM Na-citrate (3 min). Results are presented as average ± standard deviation (n=8). Significant differences were found in softened hydrogels as compared to control (*p<0.0001). C) Hydrogels stiffening (50 mM $CaCl_2$, 3 min) followed by softening (25mM Na-citrate, 3 min). Data is presented as mean ± stdev (n=3 or 2 in the case of the $CaCl_2$) (*p=0.0004). D) Hydrogels submitted to the opposite cycle i.e. softening plus stiffening. Data is presented as mean ± stdev (n=3 or 2 in the case of Na-citrate) (* p=0.0041 and **p=0.0361). E) Hydrogels stiffening was also performed with 50 mM $SrCl_2$ for 3 min (*p<0.0001, n=3).

A stiffening/softening cycle was then tested (Figure 7). As expected, treating hydrogels with 50 mM $CaCl_2$ for 3 min increased their stiffness in ca. 4.2-fold as compared to control ($p=0.0004$, Figure 8C), as previously observed. These hydrogels were then transferred to a 50 mM $CaCl_2$ for 3 min, and their stiffness decreased, returning to the original values of control hydrogels.

The opposite cycle of stiffening/softening was also tested. After softening, which resulted in a decrease of the storage modulus of ca. 2-fold as compared with the control, hydrogel's stiffness could be again increased by transferring hydrogels to 50 mM $CaCl_2$ for 3 min. In this case, the hydrogels' storage modulus was slightly higher than those of control hydrogels (ca. 1.3 fold) but in the same order of magnitude (Figure 8D).

Although $CaCl_2$ has been used as stiffening agent in previous works [100], we decided to also test here the effect of strontium ions, as calcium ions are implicated in several cellular functions, and it can be argued that changing local calcium concentration might eventually interfere with key cell signaling or cell adhesion mechanisms, for example. And, in fact, by treating hydrogels with 50 mM $SrCl_2$ (Figure 8E), we were able to obtain results similar to those obtained with calcium, with storage modulus increasing to 4244±104.10 Pa, as compared to control hydrogels (800 Pa, $p<0.0001$).

Also, in view of a future conversion of the entire system to Sr-crosslinked hydrogels, similar experiments were performed using $SrCO_3$ instead of $CaCO_3$ as internal crosslinking agent (Figure 9). The $SrCO_3$ alginate hydrogels were initially much stiffer than control $CaCO_3$ hydrogels (~2000 Pa as compared to ~800 Pa), which was expected, since alginate chains present higher affinity towards strontium [97]. When hydrogels' stiffness was further increased with 50 mM $SrCl_2$ for 3 minutes, the storage modulus reached 12510±176.80 Pa. Treatment of control hydrogels with a less concentrated 25 mM $SrCl_2$ solution was also tested. After 3 min, the storage modulus reached 8279±493.8 Pa (Figure 9A). These differences were statistical significant when compared to control ($p<0.0001$ and $p=0.0002$, respectively). It was interesting to be able to obtain two different levels of stiffness with $SrCl_2$, since using $CaCl_2$ at different concentrations and time points always resulted in similar levels of G', which were never higher than 5000 Pa. The stiffened hydrogels (25 mM $SrCl_2$, 3 min) were then transferred to 50 mM Na-citrate for 5 min and it was possible to observe a significant decrease in the storage modulus (2830±232.50 Pa) to a similar value of the control hydrogels. It is important to highlight than, in this case, treating hydrogels with 25 mM Na-citrate for 3 minutes, as in the previous assays, was insufficient to significantly decrease the stiffness of the hydrogels (data not shown). Therefore, we had to adjust the concentration of sodium citrate to 50 mM and the time of contact to 5

min.

The reverse process (softening/stiffening) was also performed (Figure 9B). After softening the hydrogels with 50 mM Na-citrate for 5 min, the storage modulus decreased to 416.4±86.68 Pa (p=0.0017, as compared to control). Subsequent stiffening with 25 mM $SrCl_2$ for 3 min increased the storage modulus to 5105±51.62 Pa (p<0.0001, as compared to control), as expected, reaching values higher than those of control hydrogels, but lower than those of hydrogels treated only with $SrCl_2$ (~8000 Pa).

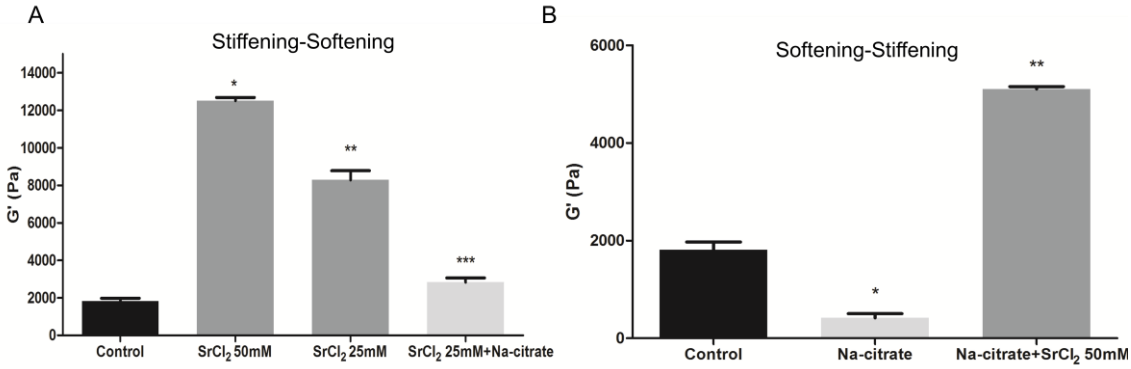

Figure 9 - Viscoelastic properties (G'-storage modulus, Pa) of Sr-alginate hydrogels submitted to stiffening and/or softening processes. (A) Stiffening was performed with two different concentrations of $SrCl_2$ (50 mM and 25 mM) and softening was performed with 50 mM Na-citrate for 5 min (*p<0.0001, **p=0.0002, ***p=0.0034). B) The opposite cycle, softening followed by stiffening, was also conducted and storage moduli were determined (* p=0.0017, **p<0.0001). Data is presented as mean ± stdev (n=3).

3.1.2. Stiffening and softening of epithelial cell-laden hydrogels

After establishing adequate conditions for the *in situ* stiffening/softening of acellular hydrogels, the knowledge was transferred to cell-laden hydrogels. In this case, only hydrogels crosslinked with $CaCO_3$ were used, to maintain the characteristics of the previously developed EMT/MET 3D model [104]. The cells used were near-normal mouse mammary epithelial EpH4 cells, which were embedded in RGD-alginate hydrogels at a concentration of 5 million cells per mL of hydrogel.

Control cell-laden hydrogels were softer than the corresponding acellular hydrogels (~360 Pa as compared to ~800 Pa). This can be explained by the fact that cells occupy a certain volume within the hydrogel network, disturbing the process of calcium-mediated binding of adjacent alginate chains and also creating defects in the network, which decreases the overall strength, and thus the storage modulus, of the hydrogels. A similar effect has been previously observed in other studies from our group [77, 110]. These hydrogels were stiffened (Figure 10) with 50 mM $CaCl_2$ for different periods of

time (3 and 10 min). Contrary to that observed for acellular hydrogels, exposure to $CaCl_2$ for distinct time periods resulted in different changes of the elastic modulus (654±52.14 Pa for 3 min, p=0.0013; and 1184±143.40 Pa for 10 min, p=0.0386, as compared to control). As the hydrogels have cells inside, the diffusion of calcium to stiffen the network can be slower, which may explain this effect. Hydrogels stiffened in 50 mM $CaCl_2$ for 10 min, were subsequently softened with 25 mM Na-citrate (Figure 11A). Yet, the 3 min used for softening acellular hydrogels were not adequate for cell-laden hydrogels, which irreversibly lost their integrity, so, in this case, 2 min were used instead, resulting in a decrease of the storage modulus to 264.7±33.99 Pa (p=0.002, as compared to control).

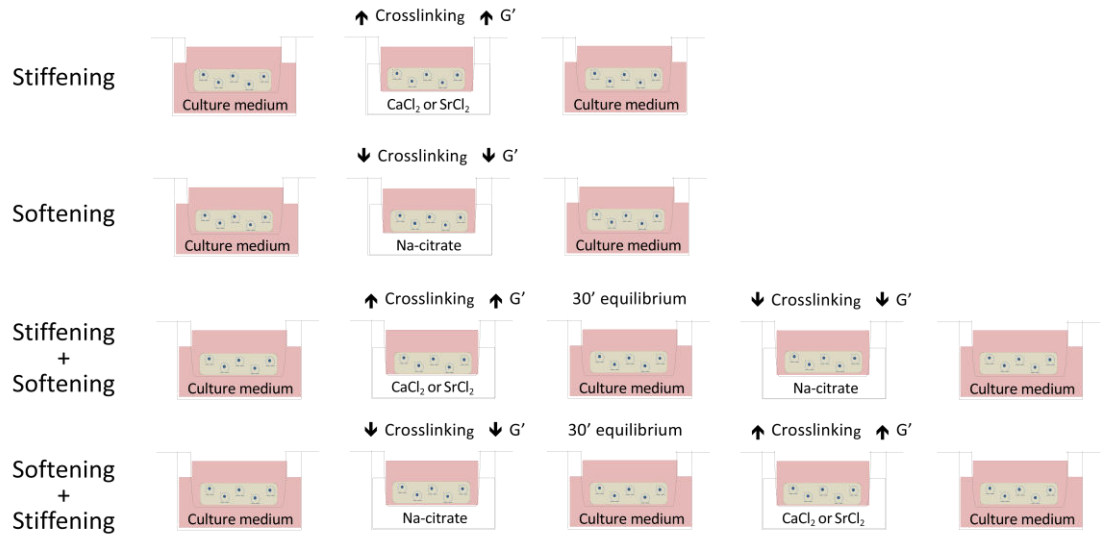

Figure 10 - Schematic representation of the process used for stiffening and/or softening EpH4-laden hydrogels.

In the case of cell-laden hydrogels, it was important to evaluate whether stiffening/softening treatments would detrimentally affect the function of entrapped cells. Evaluation of cells metabolic activity using the resazurin assay revealed that it remained high after treatment with 50 mM $CaCl_2$ for 10 min (98% of the control) and treatment with 50 mM $CaCl_2$ followed by Na-citrate, (90% of the control) (Figure 11B). Stiffening of cell-laden hydrogels with $SrCl_2$ also resulted in an increase of the storage modulus, similarly to that observed for acellular hydrogels. In this case, it was possible to obtain hydrogels with 2775±471 Pa after 10 min (p<0.0001), which could then be softened down to 1788±59.07 Pa after exposure to 50 mM Na-citrate for 5 min (p<0.0009, Figure 11C). Cells were also able to maintain high metabolic activity (Figure 11D) after treatment with $SrCl_2$ (80% of the control) and, intriguingly, the metabolic

activity attained an even higher value after a stiffening/softening a cycle of $SrCl_2$ followed by Na-citrate (97% of the control). A possible explanation for this is that softened hydrogels, which present a more permeable polymeric network, may possibly facilitate the diffusion of resazurin/resofurin during the incubation period of the metabolic activity assay, resulting in a technical artifact.

After establishing adequate conditions for stiffening cell-laden hydrogels, the next step was to optimize conditions for softening these hydrogels (Figure 10). In this case, hydrogels that were treated with 25 mM Na-citrate for 3 or even 2 min could not be handled. After 1 min of contact, the hydrogels could be recovered, but their storage moduli were almost identical to those of control hydrogels. So, new tests were performed using half of the initial concentration of Na-citrate, i.e. 12.5 mM, for 3 and 5 min. Hydrogels could be handled after both time points, and their storage moduli was quite similar, ca. 300 Pa. Statistical differences as compared to control hydrogels were only observed for the 3 min treatment ($p=0.0355$), and so this condition was selected for further experiments. Subsequent stiffening with 50 mM $CaCl_2$, resulted in only a small increase in the storage modulus (from ~300 Pa to 479.5±59.13 Pa), but upon treatment of softened hydrogels with 50mM $SrCl_2$, their storage modulus increased to 3013±632.80 Pa ($p=0.0023$, Figure 9E). This different behavior might be partially explained by the higher affinity of alginate chains to strontium vs. calcium ions, which might favor a faster and more efficient hydrogel strengthening.

Exposure to Na-citrate decreased epithelial cells metabolic activity to approximately 73% of control hydrogels (Figure 9F). This was not totally unexpected, since Na-citrate sequesters some of the crosslinking calcium ions, opening/relaxing the network and, consequently, some cells will probably be released into the culture medium during the process. Likewise, the same occurred when cells were submitted to softening/stiffening cycle both with strontium or calcium (67% and 65%, respectively). This assumption was further confirmed by normalizing cell metabolic activity results in relation to the total amount of protein present in cells recovered from the matrix, which yielded values closer to ones of control hydrogels (the average RFU/µg total protein was 35±0.86 for controls, 24.91±2.05 for softened hydrogels and 20.75±5.73 for softened/stiffened hydrogels, data not shown).

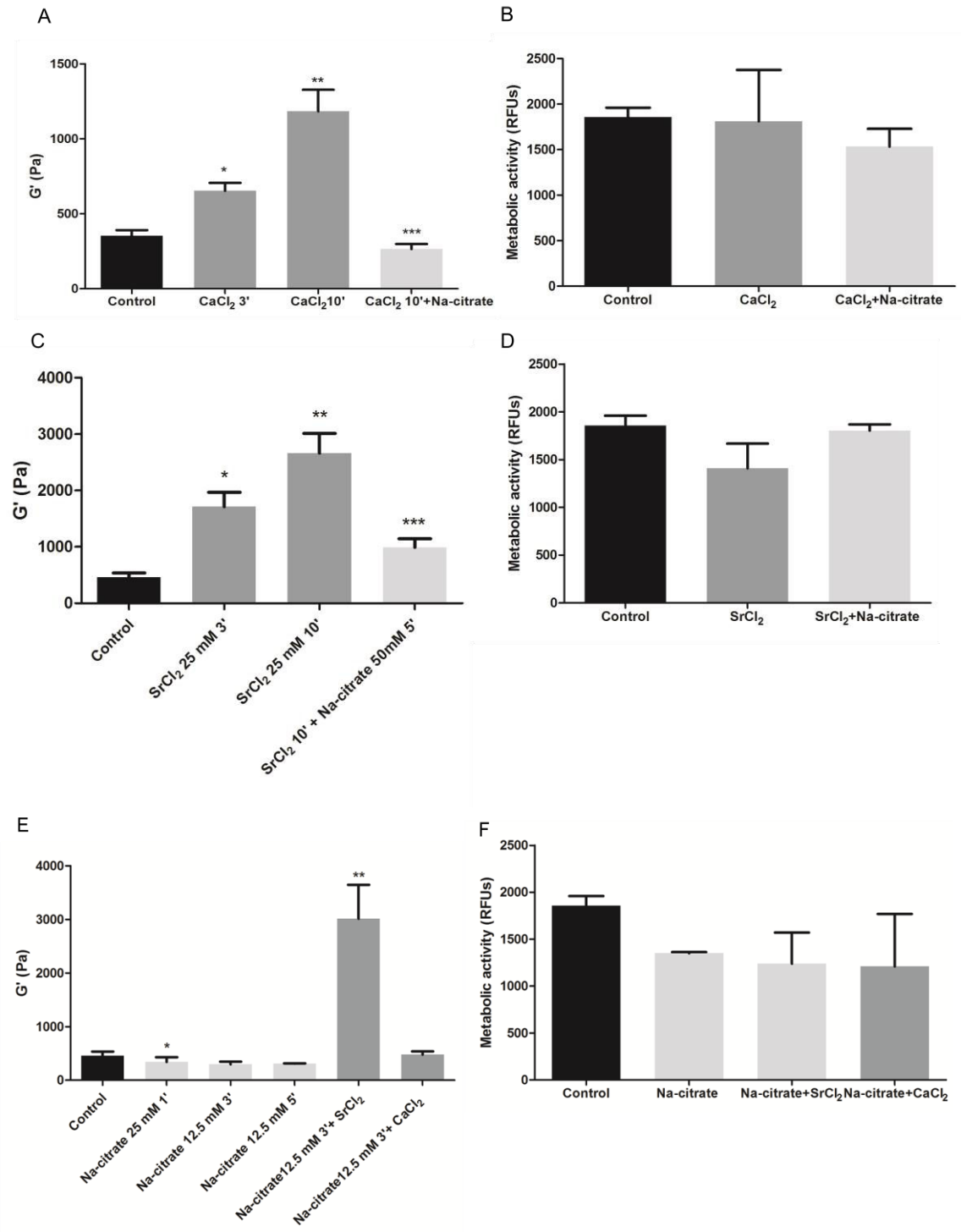

Figure 11 - Viscoelastic properties (G'-storage modulus, Pa) of Ca-alginate hydrogels with EpH4 cells entrapped submitted to stiffening and/or softening processes. (A) Stiffening was performed with 50 mM $CaCl_2$ (3 and 10 minutes) followed by softening with 25 mM Na-citrate for 2 min (*p=0.0013, **p=0.0386, *** p=0.002). C) Stiffening was also performed with 50 mM $SrCl_2$ for 3 and 10 minutes and softening was consequently executed with 50 mM Na-citrate for 5 minutes (*p=0.0009, **p<0.0001). E) Softening was performed with 25 mM Na-citrate for 1 minute and with 12.5 mM Na-citrate (3 and 5 minutes). The cycle softening-stiffening was carried out with both 50 mM $SrCl_2$ and $CaCl_2$ for 10 minutes (*p=0.0355, **p=0.0023). Metabolic activity (RFUs) was measured for the extreme conditions used (B, D, F). Data is presented as mean ± stdev (n=3 for each condition).

3.2. 3D culture in soft RGD-alginate matrices preserves the epithelial phenotype of normal mammary EpH4 cells and promotes epithelial morphogenesis

Soft alginate hydrogels functionalized with cell-adhesion RGD peptides were used in this study to simulate the 3D microenvironment of normal breast tissue. Normal murine mammary epithelial EpH4 cells, which typically assume a polygonal or cuboidal shape in 2D monolayer culture (Figure 12A), formed multicellular spheroids with high cell viability when entrapped in RGD-alginate hydrogels (Figure 12A and B). This is consistent to other studies described in the literature, which demonstrated the ability of epithelial cells to grow in 3D and form spherical clusters [48, 111, 112]. The presence of cell adhesion RGD ligands in the matrix, at a density (200 µM) similar to that of common ECM-derived biological matrices [106], was essential, leading to higher cell metabolic activity (Figure 12C) and formation of more and larger spheroids. The compliance (G'≈ 200 Pa) of the selected artificial 3D matrix was comparable to that of normal mammary tissue [49, 113, 114], and its viscoelastic properties remained unchanged along the culture period (Figure 12D), as demonstrated by rheometry analysis of cell-laden 3D matrices.

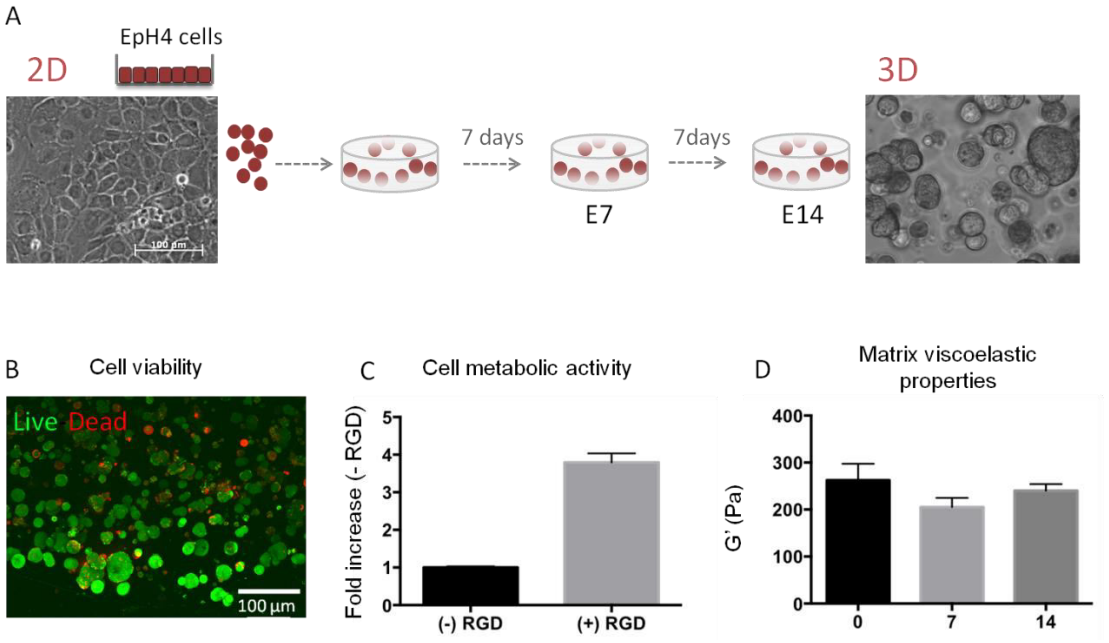

Figure 12 - Schematic representation of the established 3D *in vitro* model. A) Normal mammary epithelial cells (EpH4), were immobilized within 1 wt.% alginate matrix biofunctionalized with 200 µM RGD. To study epithelial morphogenesis, cells were kept in standard culture medium during 14 days (E cells). Bright field microscopy images of EpH4 cells in 2D (tissue culture polysytere) and 3D (RGD-alginate matrix) after 14 days of culture. B) Live/dead assay performed in 3D-cultured EpH4 cells at day 14 revealed the presence of cellular aggregates composed mostly by live cells (green, calcein staining) with few isolated dead cells (red, ethidium homodimer-1). C) Metabolic activity of EpH4 cultured in 3D alginate matrices with (+) and without (-) RGD peptides (200 µM) after 7 days in culture. D) Viscoelastic properties (storage modulus, G') of 1 wt.% RGD-alginate with EpH4 cells during 14 days of culture. Data is presented as mean ± stdev (n=3).

Immunodetection of proliferative cells (Ki67 proliferation marker) showed that EpH4, which were initially distributed as single cells within the 3D matrices, were able to proliferate, generating spheroids. At day 1, Ki-67 staining depicted proliferation in individual cells, but at days 7 and 14 proliferative cells were essentially restricted to spheroids (Figure 13A). The analysis of mitochondrial metabolic activity (Figure 13B) showed a significant increase along the first week of culture, suggesting that cells were actively proliferating, while from day 7 to day 14 no significant differences were observed, suggesting growth arrest. As time progressed, spheroids size increased reaching an average diameter of 30 µm at day 14 (Figure 13C and D).

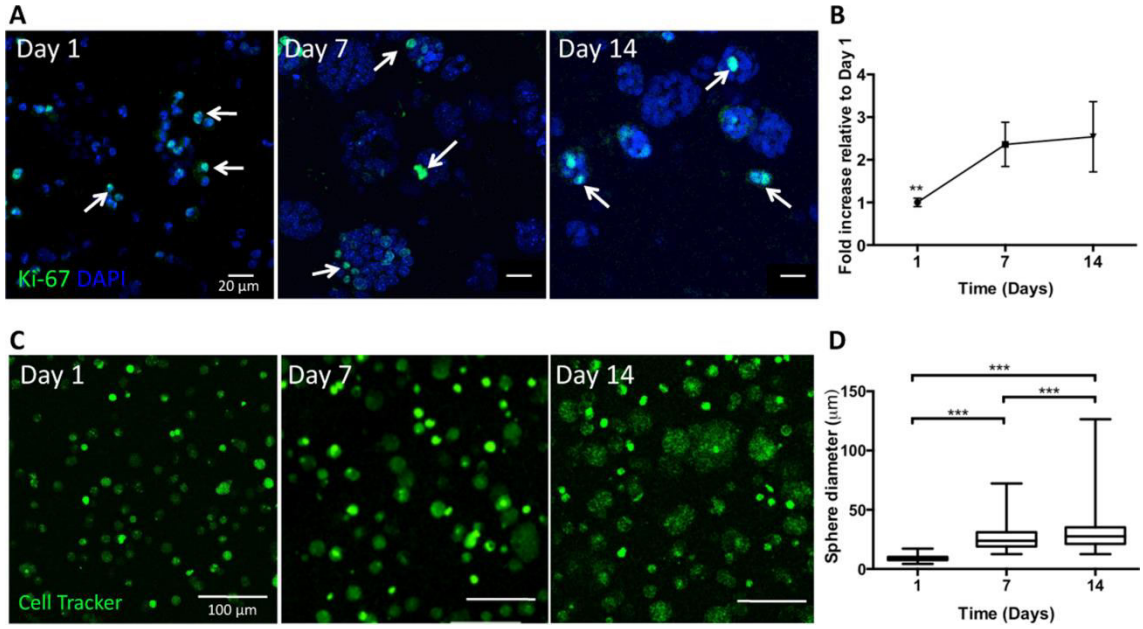

Figure 13 - Behavior of normal mammary EpH4 epithelial cells within an artificial 3D RGD-alginate matrix. A) Proliferating epithelial cells (Ki-67 positive cells, arrows) were detected within the matrix at all time points (scale bars: 20 µm). B) The metabolic activity profile showed a significantly increase after 1 week of culture. C) EpH4 cells (labeled with CellTracker™ green) formed spheroids that increased in size and number along 14 days of culture (scale bar: 100 µm). D) After 14 days of culture, spheroids reached an average diameter of 20 µm. Data is presented as mean ± stdev (n=3). Statistical significance, **p<0.01, ***p<0.001.

After 10-14 days in culture, actin-staining of EpH4-laden hydrogels revealed the formation of uniform spheroids (Figure 14A). The larger spheroids showed central clearing and lumen formation, surrounded by an organized layer of single cells reminiscent of the breast acini (Figure 14C and D).These structures showed peripheral nuclear alignment and apical-basal polarity maintained by the precise arrangement of actin filaments [115], namely at interior luminal surface and at cell-cell junctions. Similar behaviours have also been described in the literature, for instance, for MCF10A epithelial cells entrapped within a 3D matrix (composed of an interpenetrating network

of alginate and reconstituted basement membrane), which also formed typical mammary acinar structures with growth arrest, lumen formation and apicobasal polarization [111]. These structures also stained positively for functional E-cadherin (Figure 14B), a prototypical epithelial marker, which was localized at the cell membrane, stabilizing cell-cell contacts within spheroids.

By qRT-PCR, we assessed the mRNA expression of epithelial markers, *CDH1* (encoding E-cadherin) and *Ocln* (encoding Occludin); mesenchymal marker *CDH2* (encoding N-cadherin); and transcription factor *Zeb2*, a well-known EMT inducer (Figure 14E). None of the assessed markers were significantly altered across time, suggesting that 3D culture within RGD-alginate hydrogels preserves EpH4 cells epithelial phenotype and supports normal epithelial morphogenesis. This is also in accordance with the literature. For example, in one study with SCp2 cells, soft substrate with elastic modulus similar to that of normal mammary tissue were also found to be protective against EMT [112].

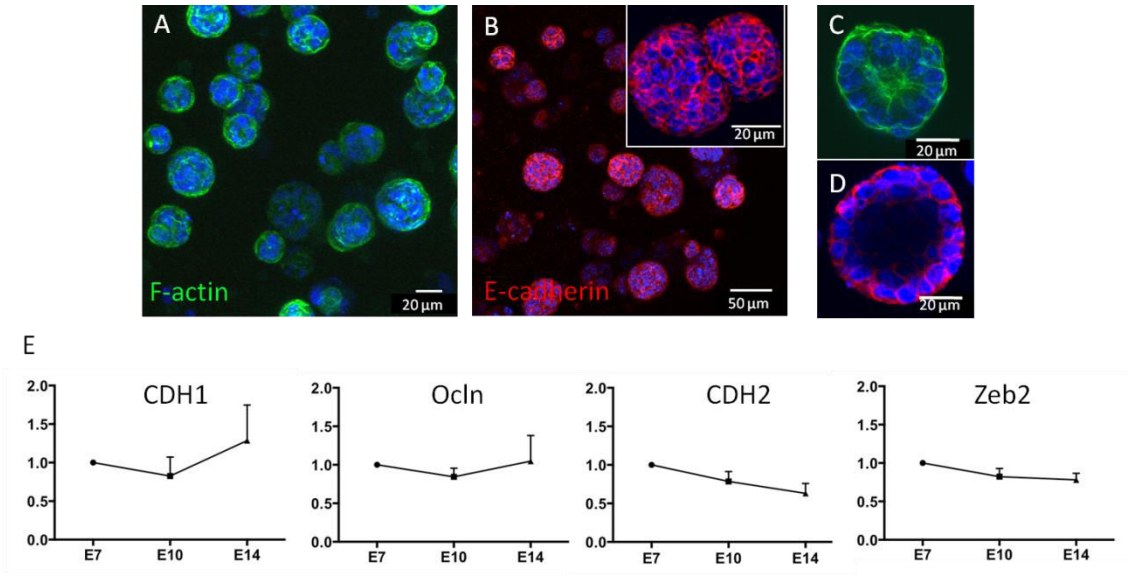

Figure 14 - Culture in RGD-alginate 3D matrix supports epithelial morphogenesis. CLSM images of 3D-cultured epithelial cells at day 14, showing: A) spheroids formation; with C and D) lumenization; and B and D) expression of the classical epithelial marker E-cadherin. Cell nuclei: blue, F-actin: green, E-cadherin: red. Scale bars (A, C, D and inset image in B): 20 µm, B): 50 µm. E) qRT-PCR quantification of relative mRNA expression of *CDH1* and *Ocln* (E markers), *CDH2* (M marker) and *Zeb2* (EMT inducer). Expression of the different markers was not significantly altered during the 14 days of culture. Data was normalized for E cells and presented as mean ± standard deviation (n=4 biological replicas).

3.3. Effect of *in situ* matrix stiffening on the behaviour of EpH4 cells cultured under 3D conditions in soft RGD-alginate matrices

After demonstrating that soft RGD-alginate hydrogels provide an adequate environment for normal epithelial morphogenesis, and do not promote EMT *per se*, the effect of *in situ* matrix stiffening on 3D cultured EpH4 cells was evaluated. The stiffening process was further optimized in this set of experiments, by increasing the concentration of the $SrCl_2$ solution from 50 mM to 100 mM (Figure 15A), and thus attain a level of stiffness closer to the one found in tumour microenvironments, i.e. around 4000 Pa [49].

Two experimental settings were tested, where matrices were stiffened 1 day after cell entrapment (as tested in 3.1 section), or only at day 10, after spheroids formation/maturation, which occurs around day 10 (as previously observed in section 3.2 and in Figure 15B). As seen in Figure 15C, the higher level of stiffening did not detrimentally affect cellular metabolic activity which remained constant and comparable to the control along 1 week of culture. Therefore, subsequent experiments were made using 100mM $SrCl_2$ as stiffening agent.

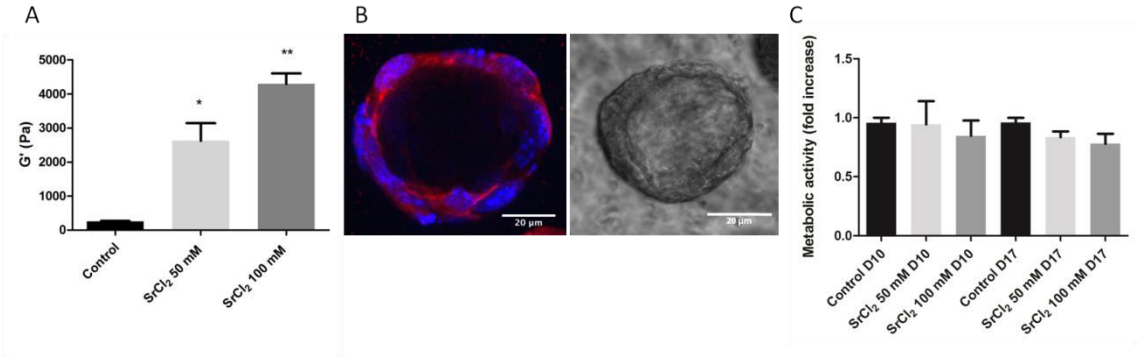

Figure 15 - Cell-laden alginate hydrogels stiffened with different concentrations of $SrCl_2$ and cellular metabolic activity. A) Stiffening was performed with both 50mM and 100mM $SrCl_2$ for 10 minutes (*p=0.0013, **p<0.0001). B) At day 10, large spheroids showed central clearing and lumen formation, surrounded by an organized layer of single cells reminiscent of the breast acini (scale bar 20 µm) and express the classical epithelial marker E-cadherin. Cell-laden hydrogels were stiffened at this time point, and maintained in culture under stiffened conditions for 7 days. C) Metabolic activity was measured in cell-laden matrices at day 10 (immediately after stiffening) and at day 17 (after 7 days in culture); the data is expressed as fold increase relative to control matrices at day 10. Data is represented as mean ± stdev (n=3).

In the first set of experiments, where cell-laden matrices were stiffened at day 1 cellular metabolic activity increased from day 1 to day 7, in control matrices, as observed in the previous section. However, in stiffened matrices, the metabolic activity increased in the first 3 days of culture, but at day 7, the value decreased, suggesting some growth

arrest (Figure 16A). Results from total protein quantification of the same samples were in agreement with those of metabolic activity assay (Figure 16B). DNA quantification showed a different result, as the values increased from day 1 to 7 in both conditions (Figure 16C). Yet, data from stiffened matrices at day 7 were not very consistent, having high standard deviations, and so these experiments must be repeated to yield conclusive results.

Spheroids formation was observed at day 7 in both control and stiffened matrices (Figure 16D). Their diameter was measured and statistical significant differences were found between the two conditions ($p<0.0001$, Figure 16E). Spheroids in control matrices had an average diameter of 60 µm, while spheroids in stiffened matrices had an average diameter of approximately 30 µm. An explanation for the observed results is still unclear. On one hand, matrix stiffness in itself may be interfering with normal epithelial morphogenesis and/or inducing phenotypic alterations, as previously described in other 3D models [111]. On the other hand, the observed differences in terms of spheroids size are also likely to be related with the more restrictive network of the stiffened matrices, which may provide a physical barrier for clonal cell growth.

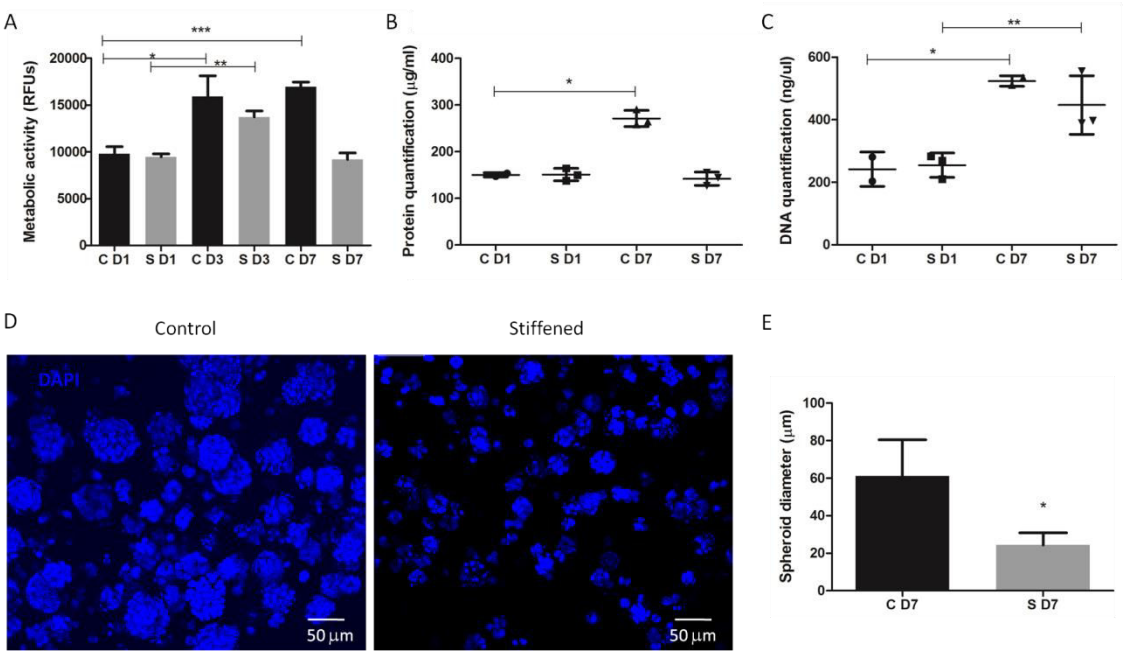

Figure 16 - Cell-laden alginate hydrogels stiffened at the first day of culture. A) Metabolic activity (RFUs) from control (C) and stiffened (S) matrices at day 1 (D1), day 3 (D3) and day 7 (D7) (*p=0.036, **p=0.001 and ***p=0.0005). B) Protein quantification was measured for the conditions depicted above (*p=0.0028). C) DNA quantification was also performed (*p=0.02 and **p=0.03). D) Spheroids were visualized with DAPI staining (scale bar 50 µm) and their diameters were measured at day 7 for both conditions (E) (*p<0.0001, n=60). Data is presented as mean ± stdev with triplicates for each condition, except in the case of C D1 and C D7 DNA quantification where only two replicates were used.

Phenotypic analysis was also performed to check the expression of with typical E and M markers, at protein level, namely E-cadherin and Vimentin, respectively (Figure 17A and B). At day 7, cell spheroids in control matrices, expressed high levels of E-cadherin, which was localized at the cellular membrane, where it promotes cell-cell adhesion. However, in stiffened matrices E-cadherin staining was less pronounced, being absent in some spheroids and/or not always present at the cellular membrane with some apparent delocalization into the cytoplasm. Vimentin expression, on the other hand, was almost absent in control samples and slightly increased in stiffened matrices. The observed decrease of the tested E marker and concomitant increase in the M marker suggests that the increase in matrix stiffness has some effect in 3D cultured epithelial cells.

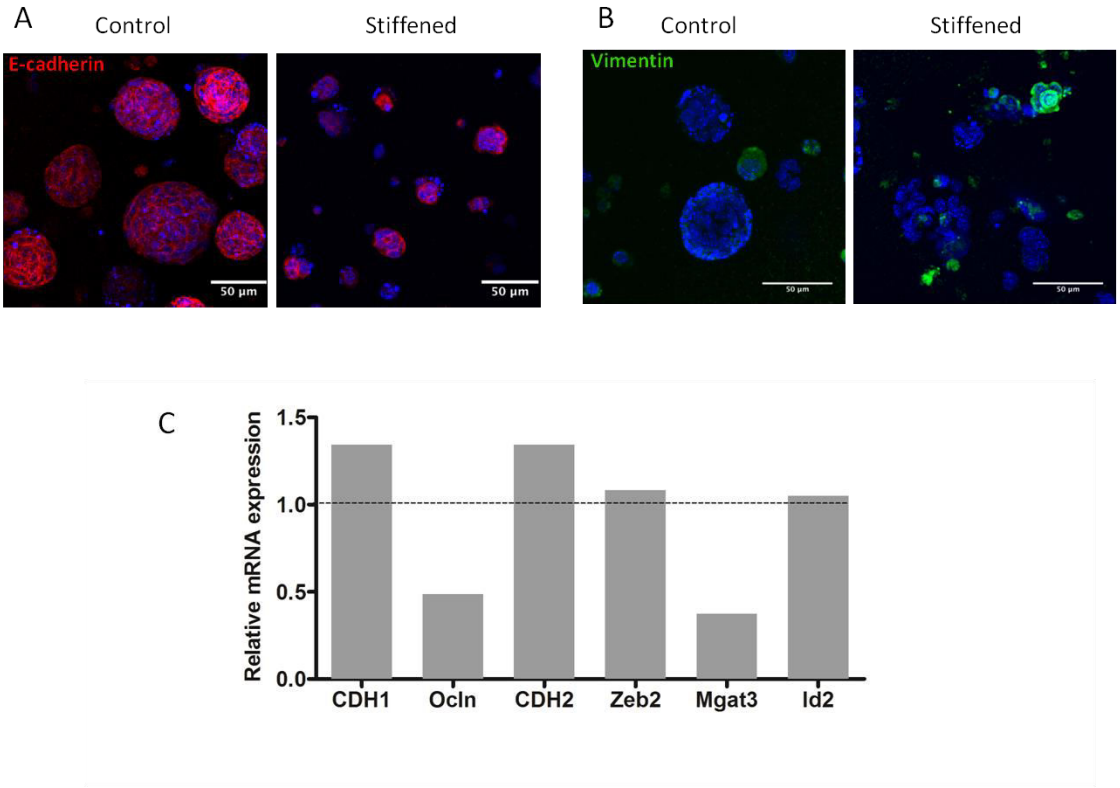

Figure 17 – EMT related markers expression at protein and mRNA levels in control and stiffened 3D matrices. A) E-cadherin expression (red, E marker) in control vs stiffened matrices (scale bar 50 µm). B) Vimentin (green, M marker) expression also in control vs stiffened matrices (scale bar 50 µm). Nuclei are counterstained in blue (DAPI). C) mRNA expression of EMT-related markers by RT-PCR (*CDH1*, *Ocln* – E; *CDH2* - M; *Zeb2* – EMT inducer; *Mgat3*, *Id2* – epithelial-associated markers) in stiffened matrices normalized to control matrices for each marker.

To better clarify this, we also analysed the mRNA expression of some EMT-related markers by qRT-PCR, namely of *CDH1* (encoding E-cadherin, E marker), *Ocln*

(encoding occluding, E marker), *CDH2* (encoding N-cadherin, M marker), *Zeb2* (EMT inductor), *Mgat3* (associated with loss of E-cadherin function [45, 101]) and *Id2* (inhibitor of differentiation 2, considered as a key negative regulator of EMT). When comparing stiffened cell-laden matrices with control ones after 7 days of culture (Figure 17C), it can be concluded that mRNA expression of *CDH1* was increased in stiffened samples, even if E-cadherin function seems to be impaired as suggested by its expression pattern at protein level. Interestingly, a similar result has been previously observed in our TGFβ1-induced EMT/MET 3D model [104]. Yet, expression of *Ocln,* another important E marker was downregulated. Expression of *CDH2* encoding the mesenchymal proteins N-cadherin, and of transcriptional factor *Zeb2* were both slightly increased in stiffened vs. control matrices. We also observed a significantly down-regulation in mRNA expression of *Mgat3*, as in our previous 3D model [104]. *Mgat3* encodes for N-acetylglucosaminyltransferase III (GnT-III), which modulates the glycation state of E-cadherin in epithelial adherens-junctions, leading to E-cadherin internalization and disruption of cell-cell contacts [45, 116]. It has been previously shown that *Mgat3* expression was dramatically decreased during EMT in 2D, and later recovered when cells partially returned to an epithelial-like phenotype, and therefore *Mgat3* glycogene (and GnT-III mediated glycosylation, specifically on E-cadherin) has been identified as novel and major component of the EMT mechanism signature. On the other hand, *Id2* is a member of the helix-loop-helix (HLH) protein family that has been described as an EMT antagonist, maintaining epithelial differentiation. Strong suppression of *Id2* expression has been observed during EMT in different epithelial models, and forcing *Id2* expression in mesenchymal cells has been shown partially rescue an epithelial phenotype [117-120]. Yet, although a significant decrease in *Id2* expression has been observed in our previous TGFβ1-induced EMT/MET 3D model, no differences between control and stiffened matrices were detected here. So, although some phenotypic alterations were detected in E cells cultured in stiffened vs. controlled matrices, eventually suggesting partial transition to a more M-like state, it must be highlighted that these experiments are still very preliminary, referring to only one biological replicate. Therefore, no solid conclusions on EMT occurrence can be taken at this stage.

The second set of experiments, where the stiffening was only performed after the formation of lumenized spheroids (day 10) revealed different results. Cellular metabolic activity levels remained nearly constant from day 10 to 17 and were similar for both conditions (Figure 18A). Also, no statistical differences were found in terms of total

protein or dsDNA quantification (Figure 18 and C), and differences in spheroids size was also much less pronounced between the two conditions (Figure 18D).

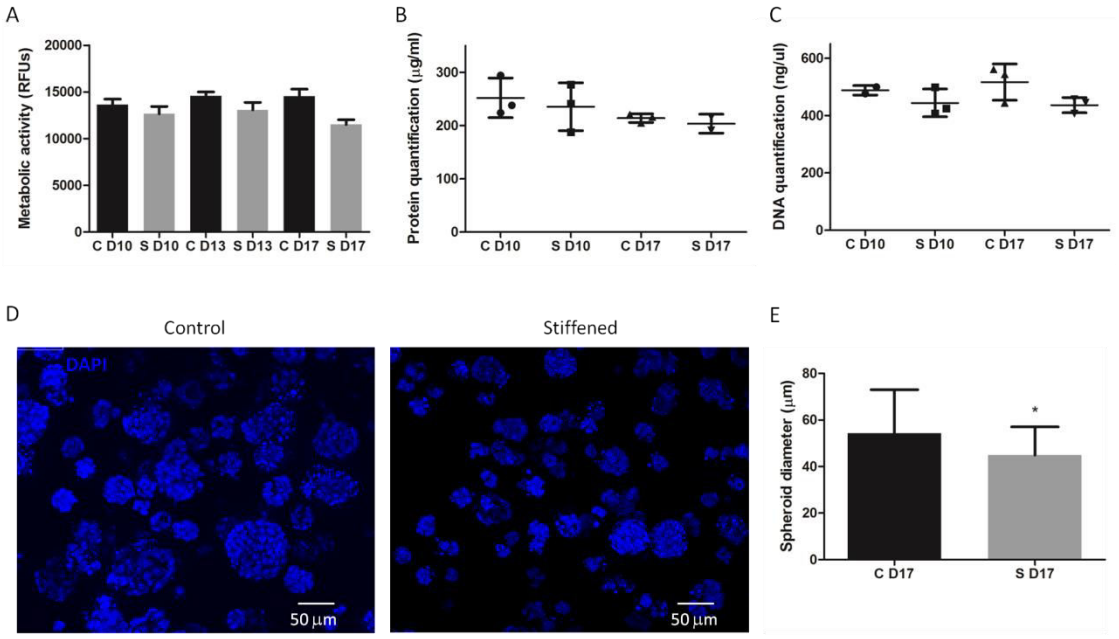

Figure 18 - Cell-laden alginate hydrogels stiffened after 10 days of culture, to allow spheroid formation. A) Metabolic activity (RFUs) from control (C) and stiffened (S) matrices at day 10 (D10), day 13 (D13) and day 17 (D17). B) Protein quantification and DNA quantification (C) were measured for the conditions depicted above. D) Spheroids were visualized with DAPI staining (scale 50 µm) and their diameters were measured at day 17 for both conditions (E) (*p<0.0001, n=60). Data is presented as mean ± stdev with triplicates for each condition, except in the case of S D17 and C D10 protein and DNA quantification, respectively, where only two replicates were considered.

Likewise, in terms of phenotypic markers, although some small differences were detected between control and stiffened matrices at protein expression level, with apparent lower expression of E-cadherin and higher expression of Vimentin (Figure 19A and B), no consistent differences were detected at mRNA expression levels (Figure 19C).

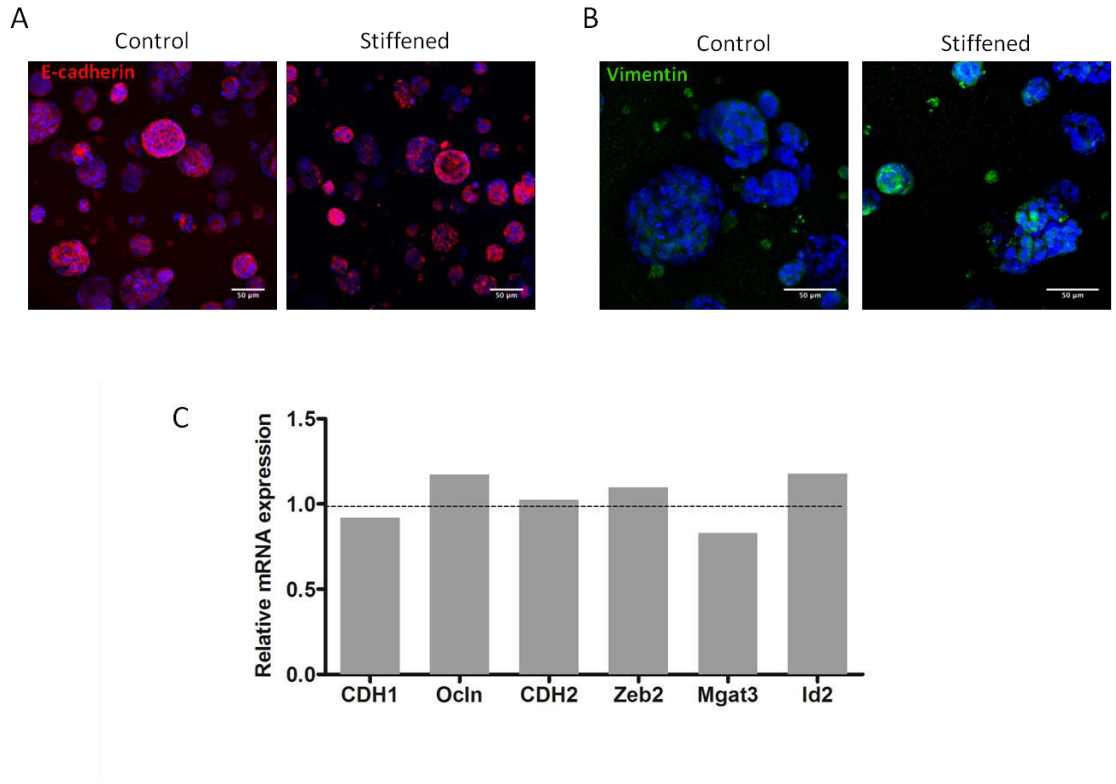

Figure 19 - Epithelial and mesenchymal markers expression in cell-laden matrices stiffened after 10 days of culture. A) E-cadherin expression (red, E marker) in control vs stiffened matrices (scale bar 50 μm). B) Vimentin (green, M marker) expression also in control vs stiffened matrices (scale bar 50 μm). DAPI is counterstained in blue (nucleus). C) E and M markers gene expression by RT-PCR (*CDH1*, *Ocln* – E; *CDH2* - M; *Zeb2* – EMT inducer; *Mgat3*, *Id2* – epithelial-associated markers) in stiffened matrices normalized with control values for each marker.

Cells undergoing EMT are known to acquire a migratory phenotype and increased invasion capacity, features also seen in tumor cells that invade and metastasize. Migration and invasion are often correlated with increased levels of matrix metalloproteinases (MMP) activity [121], namely MMP2 and MMP9 which have a key role in ECM degradation [122]. In this study, we quantified the activity of MMP2 and MMP9 (Figure 20) in conditioned media from 3D cultures. Our results show that while in the first set of experiments (matrices stiffened at day 1) the activity of both MMP2 and MMP9 slightly increased from day 1 to day 7, no differences were found between control and stiffened samples. In the second set of experiments (matrices stiffened at day 10), no differences were observed between the different time points and the different conditions. Yet, unfortunately, it was not possible to repeat this experiment, which refers to one biological replicate only, and so these results are not conclusive.

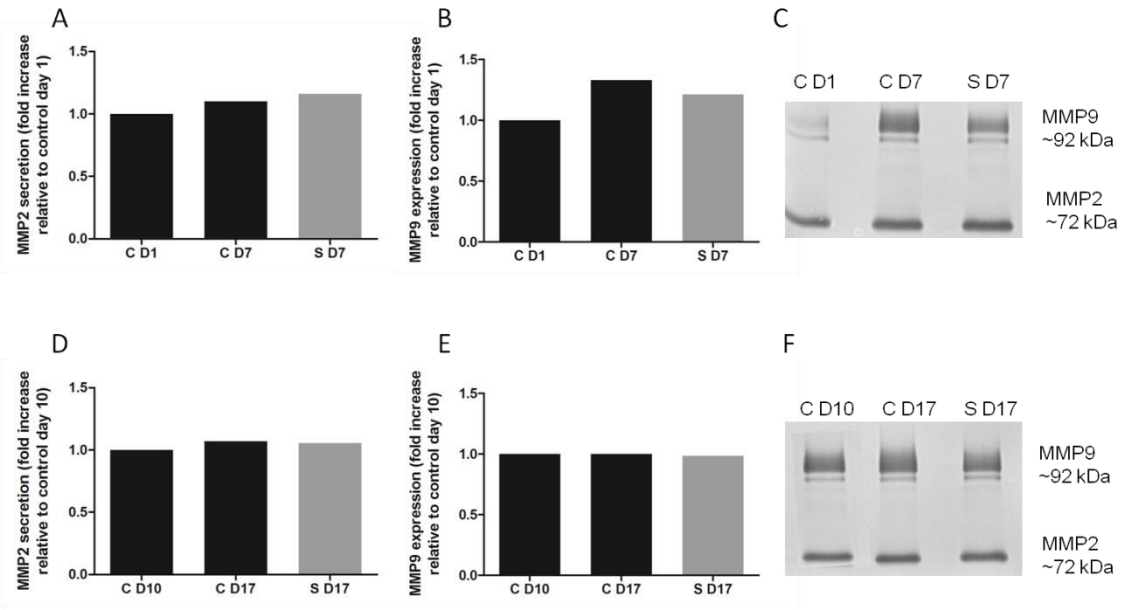

Figure 20 - MMPs secretion by cells entrapped in control or stiffened matrices. MMP2 (A) and MMP9 (B) secretion of control and stiffened cell-laden matrices at day 1 measured after 7 days in culture. The values were normalized with the MMPs secretion in control matrices at day 1 and are represented as fold increase. C) Zimogram for control matrices (day 1 and 7) and stiffened ones (day 7). MMP9 band appears at around 92 kDa and MMP2 at 72 kDa. MMP2 (D) and MMP9 (E) secretion were also analysed in matrices stiffened only after the formation of spheroids. F) Zimogram for control cell-laden matrices (day 10 and 17) and stiffened matrices (day 17).

4. Concluding Remarks and Future Perspectives

Recently, there has been a paradigm shift on cancer studies, as the role of ECM mechanical properties has started to be analysed in greater detail, appearing to play a major role on cancer progression and malignancy. In several studies where different cancer types have been analysed, from breast cancer, to prostate cancer and even brain cancers, the increased matrix rigidity surrounding the tumour seems to lead to enhanced tumour progression and poor prognosis [49, 111, 114, 123-130]. Yet, how the mechanical stimuli induce this malign progression still needs to be better clarified. In the literature, the most prevalent studies on the role of matrix stiffness on tumour progression are with epithelial cancers, with a high emphasis on breast tumours. In particular, EMT/MET transitions that occur in this type of cancer are currently also under intense investigation and have been correlated with ECM rigidity in a way that higher rigidity seems to be associated with increased malignancy.

Here, we tried to develop a new 3D *in vitro* model to help in dissecting the role of ECM-driven mechanical stimuli on EMT, taking advantage of a previous TGFβ1-induced EMT/MET 3D model previously described in the group [104]. This model was already quite useful, as compared to traditional 2D models, being more physiologically relevant and providing a closer view to the *in vivo* environment. The model is based on the use of alginate, a biocompatible and biodegradable hydrogel that mimics the ECM structure, modified with RGD peptides to promote cell-matrix adhesion. Here, the aim was to further improve these artificial microenvironments, to allow the dynamic tuning of their mechanical properties “on demand”, and precisely modulate cell-matrix interactions in a systematic way.

Using the original 3D model, we designed a protocol to alter the mechanical strength *in situ*, by stiffening the matrix with $CaCl_2$ or $SrCl_2$ and softening with sodium citrate. Interestingly, we were also able to set-up mechanical cycles where the same hydrogel could be stiffened and then softened, and *vice versa*. When epithelial EpH4 cells were entrapped in the hydrogels, the same processes could be promoted, without detrimentally affect cell behaviour. We then validated the model as an adequate microenvironment for the culture of mammary epithelial cells, showing that epithelial morphogenesis could be recapitulated with 3D cultured EpH4, which preserved their epithelial phenotype when the hydrogel stiffness was close to the one of normal breast tissue [49]. Finally, using the optimized *in situ* stiffening technique, we wanted to investigate the effect of matrix mechanical properties on epithelial cell behaviour,

namely to see if increasing matrix stiffness to values close to the ones of mammary tumour tissue [49] could, *per se*, induce EMT without further exogenous stimuli. Matrix stiffening was promoted at day 1 or 10 of culture, before and after epithelial spheroids formation, respectively. In the first set of experiments (stiffening at day 1), we were actually able to detect some phenotypic alterations in E cells cultured in stiffened vs. controlled matrices, eventually suggesting partial transition to a more M-like state. Yet, there was not enough time to repeat these experiments, and so no solid conclusions on EMT occurrence can be taken at this stage. Future studies should be focused on the repetition of these experiments, using an increased number of replicates, especially for the case of qRT-PCR and MMPs analysis.

Many other relevant aspects could be further investigated in the future using the proposed 3D model. For example, while the studies described herein were focused on the effect of matrix stiffness alone, it will be interesting, based on results from the literature, to study the potentially synergistic effects of concomitantly using other well-described EMT inducers such as TGFβ1 or even MMP3 [48].

Moreover, we could try to first induce the transition of E cells along EMT/MET with TGFβ1 as described in our previous model [104], to generate cells in the other states (i.e. mesenchymal-like cells and reverted epithelial cells), and evaluate the effect of matrix stiffness on those stages. Studying the effect of matrix stiffening/softening cycles along EMT/MET would also be quite relevant.

Our 3D model would also benefit from a parallel study using other cell lines, namely cells with cancerous background to compare with our results on near-normal epithelial cells, and the use of human derived cell lines should also be an asset. As already described, in future studies the entire system could also be converted into a “calcium-free” system, using exclusively strontium as crosslinking agent, as calcium ions are implicated in several key cellular functions.

5. References

[1] Kalluri R, Weinberg RA. The basics of epithelial-mesenchymal transition. The J Clinical Invest. 2009;119:1420-8.

[2] Tomaskovic-Crook E, Thompson EW, Thiery JP. Epithelial to mesenchymal transition and breast cancer. Breast Cancer Res. 2009;11:213-.

[3] Yang J, Weinberg RA. Epithelial-Mesenchymal Transition: At the Crossroads of Development and Tumor Metastasis. Dev Cell. 2008;14:818-29.

[4] Thiery JP. Epithelial-mesenchymal transitions in tumour progression. Nat Rev Cancer. 2002;2:442-54.

[5] Kalluri R, Weinberg RA. The basics of epithelial-mesenchymal transition. J Clinical Invest. 2009;119:1420-8.

[6] Huang X, Hang R, Wang X, Lin N, Zhang X, Tang B. Matrix stiffness in three-dimensional systems effects on the behavior of C3A cells. Artif Organs. 2013;37:166-74.

[7] Brabletz T. EMT and MET in Metastasis: Where Are the Cancer Stem Cells? Cancer Cell. 2012;22:699-701.

[8] Tsai JH, Donaher JL, Murphy DA, Chau S, Yang J. Spatiotemporal regulation of epithelial-mesenchymal transition is essential for squamous cell carcinoma metastasis. Cancer Cell. 2012;22:725-36.

[9] Aroeira LS, Aguilera A, Sanchez-Tomero JA, Bajo MA, del Peso G, Jimenez-Heffernan JA, et al. Epithelial to mesenchymal transition and peritoneal membrane failure in peritoneal dialysis patients: pathologic significance and potential therapeutic interventions. Journal of the American Society of Nephrology : JASN. 2007;18:2004-13.

[10] Palena C, Fernando RI, Hamilton DH. An immunotherapeutic intervention against tumor progression: Targeting a driver of the epithelial-to-mesenchymal transition. Oncoimmunology. 2014;3:e27220.

[11] Chui MH. Insights into cancer metastasis from a clinicopathologic perspective: Epithelial-Mesenchymal Transition is not a necessary step. Int J Cancer. 2013;132:1487-95.

[12] Principe DR, Doll JA, Bauer J, Jung B, Munshi HG, Bartholin L, et al. TGF-beta: duality of function between tumor prevention and carcinogenesis. J Natl Cancer Inst. 2014;106:djt369.

[13] Wendt MK, Allington TM, Schiemann WP. Mechanisms of the epithelial-mesenchymal transition by TGF-beta. Future oncology (London, England). 2009;5:1145-68.

[14] Zhang H, Liu L, Wang Y, Zhao G, Xie R, Liu C, et al. KLF8 involves in TGF-beta-induced EMT and promotes invasion and migration in gastric cancer cells. J Cancer Res Clin Oncol. 2013;139:1033-42.
[15] Vittal R, Fan L, Greenspan DS, Mickler EA, Gopalakrishnan B, Gu H, et al. IL-17 induces type V collagen overexpression and EMT via TGF-beta-dependent pathways in obliterative bronchiolitis. Am J Physiol Lung Cell Mol Physiol. 2013;304:L401-14.
[16] Massague J. TGFbeta in Cancer. Cell. 2008;134:215-30.
[17] Shi Y, Massague J. Mechanisms of TGF-beta signaling from cell membrane to the nucleus. Cell. 2003;113:685-700.
[18] Elloul S, Elstrand MB, Nesland JM, Trope CG, Kvalheim G, Goldberg I, et al. Snail, Slug, and Smad-interacting protein 1 as novel parameters of disease aggressiveness in metastatic ovarian and breast carcinoma. Cancer. 2005;103:1631-43.
[19] Thiery JP, Huang R. Linking epithelial-mesenchymal transition to the well-known polarity protein Par6. Dev Cell. 2005;8:456-8.
[20] Mulholland DJ, Kobayashi N, Ruscetti M, Zhi A, Tran LM, Huang J, et al. Pten loss and RAS/MAPK activation cooperate to promote EMT and metastasis initiated from prostate cancer stem/progenitor cells. Cancer research. 2012;72:1878-89.
[21] Bourboulia D, Stetler-Stevenson WG. Matrix metalloproteinases (MMPs) and tissue inhibitors of metalloproteinases (TIMPs): Positive and negative regulators in tumor cell adhesion. Sem Cancer Biol. 2010;20:161-8.
[22] Ridley AJ. Life at the leading edge. Cell. 2011;145:1012-22.
[23] Schoumacher M, Goldman RD, Louvard D, Vignjevic DM. Actin, microtubules, and vimentin intermediate filaments cooperate for elongation of invadopodia. J Cell Biol. 2010;189:541-56.
[24] Hazan RB, Qiao R, Keren R, Badano I, Suyama K. Cadherin switch in tumor progression. Ann N Y Acad Sci. 2004;1014:155-63.
[25] Mongroo PS, Rustgi AK. The role of the miR-200 family in epithelial-mesenchymal transition. Cancer Biol Ther. 2010;10:219-22.
[26] Lamouille S, Xu J, Derynck R. Molecular mechanisms of epithelial-mesenchymal transition. Nature Rev Mol Cell Biol. 2014;15:178-96.
[27] Sahlgren C, Gustafsson MV, Jin S, Poellinger L, Lendahl U. Notch signaling mediates hypoxia-induced tumor cell migration and invasion. Proc Natl Acad Sci USA 2008;105:6392-7.
[28] Kaidi A, Williams AC, Paraskeva C. Interaction between beta-catenin and HIF-1 promotes cellular adaptation to hypoxia. Nat. Cell Biol. 2007;9:210-7.

[29] Imai T, Horiuchi A, Wang C, Oka K, Ohira S, Nikaido T, et al. Hypoxia attenuates the expression of E-cadherin via up-regulation of SNAIL in ovarian carcinoma cells. Am J Pathol. 2003;163:1437-47.
[30] Kim K, Lu Z, Hay ED. Direct evidence for a role of beta-catenin/LEF-1 signaling pathway in induction of EMT. Cell Biol. Int. 2002;26:463-76.
[31] Kobayashi W, Ozawa M. The transcription factor LEF-1 induces an epithelial-mesenchymal transition in MDCK cells independent of beta-catenin. Biochem. Biophys. Res. 2013;442:133-8.
[32] Medici D, Nawshad A. Type I collagen promotes epithelial-mesenchymal transition through ILK-dependent activation of NF-kappaB and LEF-1. Matrix Biol. 2010;29:161-5.
[33] Maier HJ, Schmidt-Strassburger U, Huber MA, Wiedemann EM, Beug H, Wirth T. NF-kappaB promotes epithelial-mesenchymal transition, migration and invasion of pancreatic carcinoma cells. Cancer Lett. 2010;295:214-28.
[34] Vincent-Salomon A, Thiery JP. Host microenvironment in breast cancer development: epithelial-mesenchymal transition in breast cancer development. Breast Cancer Res. 2003;5:101-6.
[35] Perl AK, Wilgenbus P, Dahl U, Semb H, Christofori G. A causal role for E-cadherin in the transition from adenoma to carcinoma. Nature. 1998;392:190-3.
[36] Kudo-Saito C, Shirako H, Takeuchi T, Kawakami Y. Cancer metastasis is accelerated through immunosuppression during Snail-induced EMT of cancer cells. Cancer cell. 2009;15:195-206.
[37] Berx G, Becker KF, Hofler H, van Roy F. Mutations of the human E-cadherin (CDH1) gene. Human mutation. 1998;12:226-37.
[38] Berx G, Cleton-Jansen AM, Nollet F, de Leeuw WJ, van de Vijver M, Cornelisse C, et al. E-cadherin is a tumour/invasion suppressor gene mutated in human lobular breast cancers. The EMBO journal. 1995;14:6107-15.
[39] Lombaerts M, van Wezel T, Philippo K, Dierssen JW, Zimmerman RM, Oosting J, et al. E-cadherin transcriptional downregulation by promoter methylation but not mutation is related to epithelial-to-mesenchymal transition in breast cancer cell lines. Br J Cancer. 2006;94:661-71.
[40] Ling ZQ, Li P, Ge MH, Zhao X, Hu FJ, Fang XH, et al. Hypermethylation-modulated down-regulation of CDH1 expression contributes to the progression of esophageal cancer. Int J Mol Med. 2011;27:625-35.
[41] Zhao C, Bu X. Promoter methylation of tumor-related genes in gastric carcinogenesis. Histol Histopathol. 2012;27:1271-82.

[42] Moghbeli M, Moaven O, Memar B, Raziei HR, Aarabi A, Dadkhah E, et al. Role of hMLH1 and E-cadherin promoter methylation in gastric cancer progression. J Gastrointest Cancer. 2014;45:40-7.
[43] Peinado H, Olmeda D, Cano A. Snail, Zeb and bHLH factors in tumour progression: an alliance against the epithelial phenotype? Nat Rev Cancer. 2007;7:415-28.
[44] Lilien J, Balsamo J. The regulation of cadherin-mediated adhesion by tyrosine phosphorylation/dephosphorylation of beta-catenin. Curr. Opin. Cell Biol. 2005;17:459-65.
[45] Pinho SS, Oliveira P, Cabral J, Carvalho S, Huntsman D, Gartner F, et al. Loss and recovery of Mgat3 and GnT-III Mediated E-cadherin N-glycosylation is a mechanism involved in epithelial-mesenchymal-epithelial transitions. PloS one. 2012;7:e33191.
[46] Hazan RB, Phillips GR, Qiao RF, Norton L, Aaronson SA. Exogenous expression of N-cadherin in breast cancer cells induces cell migration, invasion, and metastasis. J Cell Biol. 2000;148:779-90.
[47] Egeblad M, Nakasone ES, Werb Z. Tumors as organs: complex tissues that interface with the entire organism. Dev Cell. 2010;18:884-901.
[48] Leight JL, Wozniak MA, Chen S, Lynch ML, Chen CS. Matrix rigidity regulates a switch between TGF-beta1-induced apoptosis and epithelial-mesenchymal transition. Mol Biol Cell. 2012;23:781-91.
[49] Paszek MJ, Zahir N, Johnson KR, Lakins JN, Rozenberg GI, Gefen A, et al. Tensional homeostasis and the malignant phenotype. Cancer Cell. 2005;8:241-54.
[50] Markowski MC, Brown AC, Barker TH. Directing epithelial to mesenchymal transition through engineered microenvironments displaying orthogonal adhesive and mechanical cues. J Biomed Mater Res-A. 2012;100:2119-27.
[51] Gill BJ, Gibbons DL, Roudsari LC, Saik JE, Rizvi ZH, Roybal JD, et al. A synthetic matrix with independently tunable biochemistry and mechanical properties to study epithelial morphogenesis and EMT in a lung adenocarcinoma model. Cancer Res. 2012;72:6013-23.
[52] Wei SC, Fattet L, Tsai JH, Guo Y, Pai VH, Majeski HE, et al. Matrix stiffness drives epithelial-mesenchymal transition and tumour metastasis through a TWIST1-G3BP2 mechanotransduction pathway. Nat Cell Biol. 2015;17:678-88.
[53] Santos E, Hernandez RM, Pedraz JL, Orive G. Novel advances in the design of three-dimensional bio-scaffolds to control cell fate: translation from 2D to 3D. Trends Biotechnol. 2012;30:331-41.

[54] Maschler S, Grunert S, Danielopol A, Beug H, Wirl G. Enhanced tenascin-C expression and matrix deposition during Ras/TGF-beta-induced progression of mammary tumor cells. Oncogene. 2004;23:3622-33.
[55] Loessner D, Stok KS, Lutolf MP, Hutmacher DW, Clements JA, Rizzi SC. Bioengineered 3D platform to explore cell-ECM interactions and drug resistance of epithelial ovarian cancer cells. Biomaterials. 2010;31:8494-506.
[56] Huang YJ, Hsu SH. Acquisition of epithelial-mesenchymal transition and cancer stem-like phenotypes within chitosan-hyaluronan membrane-derived 3D tumor spheroids. Biomaterials. 2014;35:10070-9.
[57] Shibata S, Marushima H, Asakura T, Matsuura T, Eda H, Aoki K, et al. Three-dimensional culture using a radial flow bioreactor induces matrix metalloprotease 7-mediated EMT-like process in tumor cells via TGFbeta1/Smad pathway. Int J Oncol. 2009;34:1433-48.
[58] Pampaloni F, Reynaud EG, Stelzer EH. The third dimension bridges the gap between cell culture and live tissue. Nat Rev Mol Cell Biol. 2007;8:839-45.
[59] Lee GY, Kenny PA, Lee EH, Bissell MJ. Three-dimensional culture models of normal and malignant breast epithelial cells. Nat Methods. 2007;4:359-65.
[60] QGel. The Innovation of QGel. 2015.
[61] Annabi N, Tamayol A, Uquillas JA, Akbari M, Bertassoni LE, Cha C, et al. 25th anniversary article: Rational design and applications of hydrogels in regenerative medicine. Adv Mater (Deerfield Beach, Fla). 2014;26:85-123.
[62] Vats K, Benoit DS. Dynamic manipulation of hydrogels to control cell behavior: a review. Tissue Eng Part B Rev. 2013;19:455-69.
[63] Gill BJ, West JL. Modeling the tumor extracellular matrix: Tissue engineering tools repurposed towards new frontiers in cancer biology. J Biomech. 2014;47:1969-78.
[64] Fischbach C, Chen R, Matsumoto T, Schmelzle T, Brugge JS, Polverini PJ, et al. Engineering tumors with 3D scaffolds. Nat Methods. 2007;4:855-60.
[65] Marx V. Tracking metastasis and tricking cancer. Nature. 2013;494:133-6.
[66] Gombotz WR, Wee SF. Protein release from alginate matrices. Adv Drug Deliv Rev. 2012;64:194-205.
[67] Haug A, Larsen B, Smidsrod O. A study of the constitution of alginic acid by partial acid hydrolysis. Acta Chem Scand. 1966;20:183-90.
[68] Andersen T A-EP, Dornish M. 3D Cell Culture in Alginate Hydrogels. Microarrays. 2015;4:133-61.
[69] Bidarra SJ, Barrias CC, Granja PL. Injectable alginate hydrogels for cell delivery in tissue engineering. Acta Biomater. 2014;10:1646-62.

[70] Augst AD, Kong HJ, Mooney DJ. Alginate hydrogels as biomaterials. Macromol Biosci. 2006;6:623-33.
[71] Drury JL, Dennis RG, Mooney DJ. The tensile properties of alginate hydrogels. Biomaterials. 2004;25:3187-99.
[72] Bidarra SJ, Barrias CC, Barbosa MA, Soares R, Granja PL. Immobilization of human mesenchymal stem cells within RGD-grafted alginate microspheres and assessment of their angiogenic potential. Biomacromol. 2010;11:1956-64.
[73] Bidarra SJ, Barrias CC, Fonseca KB, Barbosa MA, Soares RA, Granja PL. Injectable in situ crosslinkable RGD-modified alginate matrix for endothelial cells delivery. Biomaterials. 2011;32:7897-904.
[74] Fonseca KB, Bidarra SJ, Oliveira MJ, Granja PL, Barrias CC. Molecularly designed alginate hydrogels susceptible to local proteolysis as three-dimensional cellular microenvironments. Acta Biomater. 2011;7:1674-82.
[75] Fonseca KB, Gomes DB, Lee K, Santos SG, Sousa A, Silva EA, et al. Injectable MMP-sensitive alginate hydrogels as hMSC delivery systems. Biomacromol. 2014;15:380-90.
[76] Maia FR, Barbosa M, Gomes DB, Vale N, Gomes P, Granja PL, et al. Hydrogel depots for local co-delivery of osteoinductive peptides and mesenchymal stem cells. J Control Release 2014;189:158-68.
[77] Maia FR, Fonseca KB, Rodrigues G, Granja PL, Barrias CC. Matrix-driven formation of mesenchymal stem cell-extracellular matrix microtissues on soft alginate hydrogels. Acta Biomater. 2014;10:3197-208.
[78] Maia FR, Lourenco AH, Granja PL, Goncalves RM, Barrias CC. Effect of cell density on mesenchymal stem cells aggregation in RGD-alginate 3D matrices under osteoinductive conditions. Macromol Biosci. 2014;14:759-71.
[79] Kaklamani G, Cheneler D, Grover LM, Adams MJ, Bowen J. Mechanical properties of alginate hydrogels manufactured using external gelation. J Mech Behav Biomed Mater. 2014;36:135-42.
[80] Haug A. Affinity of some divalent metals to different types of alginates. Munksgaard int publ ltd 35 norre sogade, po box 2148, dk-1016 Copenhagen, Denmark; 1961. p. 1794-&.
[81] Haug A, Smidsrod O. Selectivity of some anionic polymers for divalent metal ions. Acta chem scand. 1970;24:843-54.
[82] Kuo CK, Ma PX. Ionically crosslinked alginate hydrogels as scaffolds for tissue engineering: part 1. Structure, gelation rate and mechanical properties. Biomaterials. 2001;22:511-21.

[83] Lee KY, Mooney DJ. Alginate: properties and biomedical applications. Adv Polym Sci 2012;37:106-26.
[84] Banerjee A, Arha M, Choudhary S, Ashton RS, Bhatia SR, Schaffer DV, et al. The influence of hydrogel modulus on the proliferation and differentiation of encapsulated neural stem cells. Biomaterials. 2009;30:4695-9.
[85] Chu C, Schmidt JJ, Carnes K, Zhang Z, Kong HJ, Hofmann MC. Three-dimensional synthetic niche components to control germ cell proliferation. Tissue Eng Part A. 2009;15:255-62.
[86] Masuda K, Sah RL, Hejna MJ, Thonar EJ. A novel two-step method for the formation of tissue-engineered cartilage by mature bovine chondrocytes: the alginate-recovered-chondrocyte (ARC) method. J Orthop Res. 2003;21:139-48.
[87] Park H, Kang SW, Kim BS, Mooney DJ, Lee KY. Shear-reversibly Crosslinked Alginate Hydrogels for Tissue Engineering. Macromol Biosci. 2009;9:895-901.
[88] Penolazzi L, Tavanti E, Vecchiatini R, Lambertini E, Vesce F, Gambari R, et al. Encapsulation of mesenchymal stem cells from Wharton's jelly in alginate microbeads. Tissue Eng Part C. 2009;16:141-55.
[89] Sheng L, Leshchyns'ka I, Sytnyk V. Cell adhesion and intracellular calcium signaling in neurons. J Cell Commun Signal. 2013;11:94.
[90] Tanaka M, Ichikawa-Tomikawa N, Shishito N, Nishiura K, Miura T, Hozumi A, et al. Co-expression of S100A14 and S100A16 correlates with a poor prognosis in human breast cancer and promotes cancer cell invasion. BMC cancer. 2015;15:53.
[91] Duvivier-Kali VF, Omer A, Lopez-Avalos MD, O'Neil JJ, Weir GC. Survival of microencapsulated adult pig islets in mice in spite of an antibody response. Am J Transplant 2004;4:1991-2000.
[92] Duvivier-Kali VF, Omer A, Parent RJ, O'Neil JJ, Weir GC. Complete protection of islets against allorejection and autoimmunity by a simple barium-alginate membrane. Diabetes. 2001;50:1698-705.
[93] Omer A, Duvivier-Kali VF, Trivedi N, Wilmot K, Bonner-Weir S, Weir GC. Survival and maturation of microencapsulated porcine neonatal pancreatic cell clusters transplanted into immunocompetent diabetic mice. Diabetes. 2003;52:69-75.
[94] Schneider S, Feilen PJ, Brunnenmeier F, Minnemann T, Zimmermann H, Zimmermann U, et al. Long-term graft function of adult rat and human islets encapsulated in novel alginate-based microcapsules after transplantation in immunocompetent diabetic mice. Diabetes. 2005;54:687-93.
[95] Zekorn T, Horcher A, Siebers U, Schnettler R, Klöck G, Hering B, et al. Barium-cross-linked alginate beads: a simple, one-step method for successful immunoisolated transplantation of islets of Langerhans. Acta Diabetol. 1992;29:99-106.

[96] Smidsrod O, Haug A. Properties of Poly (l, 4-hexuronates) in the Gel State. Acta Chem Scand. 1972;26:6.
[97] Morch YA, Donati I, Strand BL, Skjak-Braek G. Effect of Ca2+, Ba2+, and Sr2+ on alginate microbeads. Biomacromol. 2006;7:1471-80.
[98] Thu B, Bruheim P, Espevik T, Smidsrod O, Soon-Shiong P, Skjak-Braek G. Alginate polycation microcapsules. I. Interaction between alginate and polycation. Biomaterials. 1996;17:1031-40.
[99] Martinsen A, Skjak-Braek G, Smidsrod O. Alginate as immobilization material: I. Correlation between chemical and physical properties of alginate gel beads. Biotechnol Bioeng. 1989;33:79-89.
[100] Gillette BM, Jensen JA, Wang M, Tchao J, Sia SK. Dynamic hydrogels: switching of 3D microenvironments using two-component naturally derived extracellular matrices. Adv Mat (Deerfield Beach, Fla). 2010;22:686-91.
[101] Oliveira P, Rocha S, Azevedo M, Vieira A, Ferreira D, Mendes N, Reis I, Vinagre J, Heravi-Moussavi A, Nunes JB, Lima J, Máximo V, Burleigh A, Roskelley C, Carneiro F, Seruca R, Paredes J, Huntsman D, Oliveira C. Through the looking glass: the reversion of EMT. European Society of Human Genetics Conference 2015.
[102] Schmidt JM, Panzilius E, Bartsch HS, Irmler M, Beckers J, Kari V, et al. Stem-cell-like properties and epithelial plasticity arise as stable traits after transient Twist1 activation. Cell reports. 2015;10:131-9.
[103] Yu M, Bardia A, Wittner BS, Stott SL, Smas ME, Ting DT, et al. Circulating breast tumor cells exhibit dynamic changes in epithelial and mesenchymal composition. Science (New York, NY). 2013;339:580-4.
[104] Bidarra SJ, Oliveira P, Saraiva D, Oliveira C, Barrias CC. A 3D in vitro model to explore the inter-conversion between epithelial and mesenchymal states during EMT and its reversion. Submitted. 2015.
[105] Rowley JA, Madlambayan G, Mooney DJ. Alginate hydrogels as synthetic extracellular matrix materials. Biomaterials. 1999;20:45-53.
[106] Huebsch N, Arany PR, Mao AS, Shvartsman D, Ali OA, Bencherif SA, et al. Harnessing traction-mediated manipulation of the cell/matrix interface to control stem-cell fate. Nat Materials. 2010;9:518-26.
[107] Oliveira SM, Barrias CC, Almeida IF, Costa PC, Ferreira MR, Bahia MF, et al. Injectability of a bone filler system based on hydroxyapatite microspheres and a vehicle with in situ gel-forming ability. J Biomed Mater Res B Appl Biomater. 2008;87:49-58.
[108] Montesano R, Soriano JV, Fialka I, Orci L. Isolation of EpH4 mammary epithelial cell subpopulations which differ in their morphogenetic properties. In Vitro Cell Dev Biol Anim 1998;34:468-77.

[109] Livak KJ, Schmittgen TD. Analysis of relative gene expression data using real-time quantitative PCR and the 2(-Delta Delta C(T)) Method. Methods (San Diego, Calif). 2001;25:402-8.
[110] Fonseca KB, Maia FR, Cruz FA, Andrade D, Juliano MA, Granja PL, et al. Enzymatic, physicochemical and biological properties of MMP-sensitive alginate hydrogels. Soft Matter. 2013;9:3283-92.
[111] Chaudhuri O, Koshy ST, Branco da Cunha C, Shin JW, Verbeke CS, Allison KH, et al. Extracellular matrix stiffness and composition jointly regulate the induction of malignant phenotypes in mammary epithelium. Nat Materials. 2014;13:970-8.
[112] Lee K, Chen QK, Lui C, Cichon MA, Radisky DC, Nelson CM. Matrix compliance regulates Rac1b localization, NADPH oxidase assembly, and epithelial-mesenchymal transition. Mol Biol Cell. 2012;23:4097-108.
[113] Butcher DT, Alliston T, Weaver VM. A tense situation: forcing tumour progression. Nat Rev Cancer. 2009;9:108-22.
[114] Levental KR, Yu H, Kass L, Lakins JN, Egeblad M, Erler JT, et al. Matrix crosslinking forces tumor progression by enhancing integrin signaling. Cell. 2009;139:891-906.
[115] Mi K, Xing Z. CD44(+)/CD24(-) breast cancer cells exhibit phenotypic reversion in three-dimensional self-assembling peptide RADA16 nanofiber scaffold. Int J Nanomedicine 2015;10:3043-53.
[116] Xu Q, Isaji T, Lu Y, Gu W, Kondo M, Fukuda T, et al. Roles of N-acetylglucosaminyltransferase III in epithelial-to-mesenchymal transition induced by transforming growth factor beta1 (TGF-beta1) in epithelial cell lines. J Biol Chem. 2012;287:16563-74.
[117] Chang C, Yang X, Pursell B, Mercurio AM. Id2 complexes with the SNAG domain of Snai1 inhibiting Snai1-mediated repression of integrin beta4. Mol Cell Biol. 2013;33:3795-804.
[118] Kondo M, Cubillo E, Tobiume K, Shirakihara T, Fukuda N, Suzuki H, et al. A role for Id in the regulation of TGF-beta-induced epithelial-mesenchymal transdifferentiation. Cell Death Differ. 2004;11:1092-101.
[119] Kowanetz M, Valcourt U, Bergstrom R, Heldin CH, Moustakas A. Id2 and Id3 define the potency of cell proliferation and differentiation responses to transforming growth factor beta and bone morphogenetic protein. Mol Cell Biol. 2004;24:4241-54.
[120] Zavadil J, Bottinger EP. TGF-beta and epithelial-to-mesenchymal transitions. Oncogene. 2005;24:5764-74.

[121] Radisky ES, Radisky DC. Matrix Metalloproteinase-Induced Epithelial-Mesenchymal Transition in Breast Cancer. J Mammary Gland Biol Neoplasia. 2010;15:201-12.
[122] Jacob A, Prekeris R. The regulation of MMP targeting to invadopodia during cancer metastasis. Front Cell Dev Biol. 2015;3:4.
[123] Ahmad S, Cao R, Varghese T, Bidaut L, Nabi G. Transrectal quantitative shear wave elastography in the detection and characterisation of prostate cancer. Surg Endosc 2013;27:3280-7.
[124] Boyd NF, Li Q, Melnichouk O, Huszti E, Martin LJ, Gunasekara A, et al. Evidence that breast tissue stiffness is associated with risk of breast cancer. PloS one. 2014;9:e100937.
[125] Fenner J, Stacer AC, Winterroth F, Johnson TD, Luker KE, Luker GD. Macroscopic stiffness of breast tumors predicts metastasis. Scientific reports. 2014;4:5512.
[126] Kaluzny J, Kopec T, Szczepanek-Parulska E, Stangierski A, Gurgul E, Ruchala M, et al. Shear wave elastography: a new noninvasive tool to assess the intensity of fibrosis of irradiated salivary glands in head and neck cancer patients. Biomed Res Int. 2014;2014:157809.
[127] Lam WA, Cao L, Umesh V, Keung AJ, Sen S, Kumar S. Extracellular matrix rigidity modulates neuroblastoma cell differentiation and N-myc expression. Mol Cancer. 2010;9:35.
[128] Li T, Sun L, Miller N, Nicklee T, Woo J, Hulse-Smith L, et al. The association of measured breast tissue characteristics with mammographic density and other risk factors for breast cancer. Cancer Epidemiol. Biomarkers Prev. 2005;14:343-9.
[129] Mouw JK, Yui Y, Damiano L, Bainer RO, Lakins JN, Acerbi I, et al. Tissue mechanics modulate microRNA-dependent PTEN expression to regulate malignant progression. Nat Med. 2014;20:360-7.
[130] Provenzano PP, Inman DR, Eliceiri KW, Keely PJ. Matrix density-induced mechanoregulation of breast cell phenotype, signaling and gene expression through a FAK-ERK linkage. Oncogene. 2009;28:4326-43.